Lysosomal targeting of the ABC transporter TAPL is determined by membrane-localized charged residues

Received for publication, December 11, 2018, and in revised form, March 8, 2019 Published, Papers in Press, March 15, 2019, DOI 10.1074/jbc.RA118.007071

Philipp Graab[‡], Christoph Bock[‡], Konstantin Weiss[‡], Alexander Hirth[‡], Nicole Koller[‡], Markus Braner[‡], Jennifer Jung[§], Frank Loehr[¶], Robert Tampé[‡], Christian Behrends[§‖], and Rupert Abele[‡1]

From the [‡]Institute of Biochemistry, Biocenter, and the [¶]Institute of Biophysical Chemistry and Center for Biomolecular Magnetic Resonance, Goethe University Frankfurt, Max-von-Laue-Strasse 9, 60438 Frankfurt am Main, Germany, the [§]Institute of Biochemistry II, Medical School, Goethe University Frankfurt, Theodor-Stern-Kai 7, 60590 Frankfurt am Main, Germany, and the [‖]Munich Cluster for Systems Neurology, Ludwig Maximilians University Munich, Feodor-Lynen-Strasse 17, 81377 Munich, Germany

Edited by Phyllis I. Hanson

The human lysosomal polypeptide ABC transporter TAPL (ABC subfamily B member 9, ABCB9) transports 6–59-amino-acid-long polypeptides from the cytosol into lysosomes. The subcellular localization of TAPL depends solely on its N-terminal transmembrane domain, TMD0, which lacks conventional targeting sequences. However, the intracellular route and the molecular mechanisms that control TAPL localization remain unclear. Here, we delineated the route of TAPL to lysosomes and investigated the determinants of single trafficking steps. By synchronizing trafficking events by a retention using selective hooks (RUSH) assay and visualizing individual intermediate steps through immunostaining and confocal microscopy, we demonstrate that TAPL takes the direct route to lysosomes. We further identified conserved charged residues within TMD0 transmembrane helices that are essential for individual steps of lysosomal targeting. Substitutions of these residues retained TAPL in the endoplasmic reticulum (ER) or Golgi. We also observed that for release from the ER, a salt bridge between Asp-17 and Arg-57 is essential. An interactome analysis revealed that Yip1-interacting factor homolog B membrane-trafficking protein (YIF1B) interacts with TAPL. We also found that YIF1B is involved in ER-to-Golgi trafficking and interacts with TMD0 of TAPL via its transmembrane domain and that this interaction strongly depends on the newly identified salt bridge within TMD0. These results expand our knowledge about lysosomal trafficking of TAPL and the general function of extra transmembrane domains of ABC transporters.

ATP-binding cassette (ABC)[2] transporters belong to one of the largest protein families in all organisms (1). In eukaryotes, they are almost exclusively exporters, transporting a diverse set of solutes across membranes while hydrolyzing ATP (2). The cytosolic nucleotide-binding domains (NBDs) translate their ATP binding–induced dimerization and subsequent ATP hydrolysis in conformational changes of the transmembrane domains (TMDs), which leads to translocation of the solute across the membrane. The common core architecture of human ABC exporters comprises 2 × 6 transmembrane helices (TMHs) and two NBDs, arranged either as a single polypeptide chain (full transporter) or as dimers (half-transporters).

In humans, 48 ABC proteins are found. A small subgroup of them forms the transporter associated with antigen processing (TAP) family, consisting of TAP1 (ABCB2) and TAP2 (ABCB3) forming a heterodimer and the homodimeric TAP-like (TAPL/ABCB9). TAPL is able to transport polypeptides varying between 6 and 59 amino acids in length (3). In contrast to ER-resident TAP, which is part of the peptide loading complex (4, 5), TAPL is localized to lysosomes (6). To date, the physiological role of TAPL remains ill-defined. It was shown that TAPL expression is strongly up-regulated after maturation of monocytes to professional antigen-presenting cells like macrophages and dendritic cells (7). However, no evidence was found for TAPL being involved in antigen cross-presentation (8). In contrast, it is associated with phagosomal maturation, consistent with earlier studies on the TAPL orthologous HAF-4 and HAF-9 of *Caenorhabditis elegans*, which are essential for gut granule biogenesis (9).

TAPL can be dissected into two functional parts (10). CoreTAPL, comprising the six C-terminal TMHs and the cytosolic NBD, forms homodimers that are fully active in ATP-dependent peptide transport. The four additional N-terminal TMHs, named TMD0, are negligible for peptide transport but essential for lysosomal localization (11) and for interaction with the lysosomal membrane proteins LAMP-1 and LAMP-2B (12). CoreTAPL, lacking the TMD0, is mislocalized to the plasma

This work was supported by German Research Foundation Grants SFB 807 (to P. G., C. Bock, N. K., R. A., and R. T.), SFB 1177 (to C. Behrends), SPP 1623 (to R. T. and M. B.), EXC1010 SyNergy (to C. Behrends), and AB149/1-2 (to R. A.); the Boehringer Ingelheim Foundation (to C. Behrends); and the Center for Biomolecular Magnetic Resonance (to F. L.). The authors declare that they have no conflicts of interest with the contents of this article.

This article contains Tables S1–S3 and Figs. S1–S12.

The MS proteomics data have been deposited to the ProteomeXchange Consortium via the PRIDE (67) partner repository with the data set identifier PXD010989.

[1] To whom correspondence should be addressed. Tel.: 49-69-79829437; Fax: 49-69-79829495; E-mail: abele@em.uni-frankfurt.de.

[2] The abbreviations used are: ABC, ATP-binding cassette; NBD, nucleotide-binding domain; TMD, transmembrane domain; TMH, transmembrane helix; c6-DHPC, 1,2-dihexanoyl-*sn*-glycero-3-phosphocholine; TAP, transporter associated with antigen processing; TAPL, TAP-like; PM, plasma membrane; TGN, *trans*-Golgi network; IP, immunoprecipitation; RUSH, retention using selective hooks; SBP, streptavidin-binding peptide; PCC, Pearson correlation coefficient; CHX, cycloheximide; HCIP, high-confidence candidate interacting protein; NP40, Nonidet P-40; eGFP, enhanced GFP; FCS, fetal calf serum; PEI, polyethyleneimine; sgRNA, single guide RNA; PSF, point-spread function; Tricine, *N*-[2-hydroxy-1,1-bis(hydroxymethyl)ethyl]glycine; IRES, internal ribosome entry site.

membrane (PM), whereas the TMD0 itself is trafficked to lysosomes. If both parts are co-expressed, coreTAPL interacts noncovalently with TMD0, which leads to lysosomal localization (11).

For lysosomal membrane proteins, two intracellular biosynthetic routes are described (13, 14). The direct route leads from the *trans*-Golgi network (TGN) via early endosomes and late endosomes to lysosomes. In contrast, the indirect route includes an intermediate trafficking step at the PM, subsequent endocytosis, and transport to early endosomes. Short linear targeting motifs determine individual trafficking steps. Most common are tyrosine (Y*XX*Φ)- or dileucine ((D/E)*XXX*L(L/I))-based motifs in a cytosolic region of the lysosomal membrane protein. These sequences are recognized by cytosolic adaptor proteins such as the five adaptor protein complexes (AP-1 to -5) or the monomeric GGAs (Golgi-localizing, γ-adaptin ear domain homology, ARF-binding proteins). None of these consensus sequences associated with protein trafficking can be found in the TMD0 of TAPL. However, an increasing body of evidence clearly demonstrates that lysosomal localization can also be mediated by atypical targeting determinants ranging from anomalous leucine or tyrosine motifs to post-translational modifications (15).

In this study, we investigated the trafficking of TAPL to elucidate the intracellular route to lysosomes, especially with regard to a possible PM intermediate step. In mutational studies, we were able to determine conserved, charged residues within TMD0 that are essential for individual trafficking steps and thus form the targeting determinants of TAPL. Immunoprecipitation-MS (IP-MS) allowed us to identify YIF1B, a factor in ER-to-Golgi trafficking, as an interaction partner of TAPL involved in the targeting process. The interaction between the two proteins is mediated by the TMD of YIF1B and TMD0 of TAPL, with significantly reduced interaction if the salt bridge between two conserved, charged residues in TMD0 is disrupted.

Results

Intracellular route of TAPL

To decipher the intracellular route of TAPL to lysosomes, we applied the retention using selective hooks (RUSH) assay (16), which enables synchronization of protein trafficking and thus visualization of intermediate steps. HeLa Kyoto cells were transiently transfected with a bicistronic plasmid. One gene coded for the invariant chain (Ii, CD74) containing an N-terminal, cytosolic ER retention signal and core streptavidin as hook, whereas the other coded for TAPL, fused C-terminally with a streptavidin-binding peptide (SBP) followed by eGFP (Fig. 1*A*). In the absence of biotin, TAPL colocalized with the hook protein, demonstrating efficient ER retention, and did not overlap with GM130 (*cis*-Golgi), EEA1 (early endosomes), and LAMP-1 (lysosomes) (Fig. S1*A*). By adding biotin, the interaction between TAPL and the hook protein was outcompeted, and TAPL was released and trafficked to lysosomes in a time-dependent manner. Within 15 min after the addition of biotin, TAPL accumulated in a perinuclear area partially overlapping with the *cis*-Golgi marker GM130, which represents the first trafficking step from ER to the Golgi (Fig. 1*B* and Fig. S1*B*). After 45–60 min, TAPL colocalization with GM130 was reduced, and a fraction of TAPL was found in distinct vesicular structures stained with the early endosomal marker EEA1. Finally, a first overlap with the late endosomal and lysosomal marker LAMP-1 was observed after 60–90 min. In this context, it should be noted that trafficking periods vary between cells dependent on cellular TAPL levels, with faster kinetics for low expressing cells. According to the observed localizations, TAPL takes an intracellular route from the ER, via Golgi and early endosomes to late endosomal and lysosomal compartments.

To exclude the possibility that we missed a short-lived PM-trafficking step that reflects the indirect route, we inhibited endocytosis by the dynamin inhibitor Dyngo-4a (17). HeLa Flp-In T-REx cells were used to allow stable, inducible expression of *tapl* under the control of the tetracycline-regulated promotor. To inhibit endocytosis during TAPL synthesis and trafficking, Dyngo-4a was added together with the inducer doxycycline. 2 h after induction, TAPL was detected in lysosomes, but no PM localization was observed (Fig. 1*C*). To verify the inhibitory function of Dyngo-4a, we analyzed the clathrin- and dynamin-dependent endocytosis of the transferrin receptor, which can be triggered by the addition of transferrin (18, 19). In the presence of Dyngo-4a, transferrin was not taken up by endocytosis, in contrast to the inactive control compound Dyngo-Ø, which did not interfere with endocytosis, as proven by immunofluorescence microscopy as well as by flow cytometry (Fig. S2). Thus, Dyngo-4a is capable of fully blocking dynamin-dependent endocytosis. Collectively, these data demonstrate that TAPL solely takes the direct route from the ER via Golgi and early endosomes to lysosomes.

Residues involved in intracellular trafficking

Intracellular trafficking steps are mediated by targeting motifs. However, none of the tyrosine- or dileucine-based motifs classically associated with lysosomal targeting are found in the cytosolic loops of TMD0, the targeting domain of TAPL. To elucidate how TMD0 mediates individual targeting steps along the intracellular route, we performed multiple sequence alignments of TAPL orthologues of phylogenetically distant species to identify conserved residues (Fig. S3).

As derived from a recently published secondary structure model of TMD0 (Fig. 2) (20), all eight conserved residues, three leucines and five charged residues found in species from humans to *C. elegans*, are localized in the transmembrane helices 1, 2, and 3. Because charged residues in the hydrophobic core of the membrane often accompany special functions, we focused our targeting studies on the charged residues Asp-17 in TMH1, Asp-49 and Arg-57 in TMH2, and Lys-100 in TMH3. The following studies were performed with HeLa and HEK cells, in which endogenous TAPL expression was detected at the mRNA level (21). However, at the protein level, endogenous TAPL could not be detected by either immunoblot or immunofluorescence microscopy, most likely due to low abundance of TAPL in these cells (7). Therefore, analysis of intracellular localization of TAPL mutants was carried out using stably transfected HeLa Flp-In T-REx cells. This system enabled mild overexpression of TAPL by means of low inducer concentrations and thus led to a more robust localization analysis across

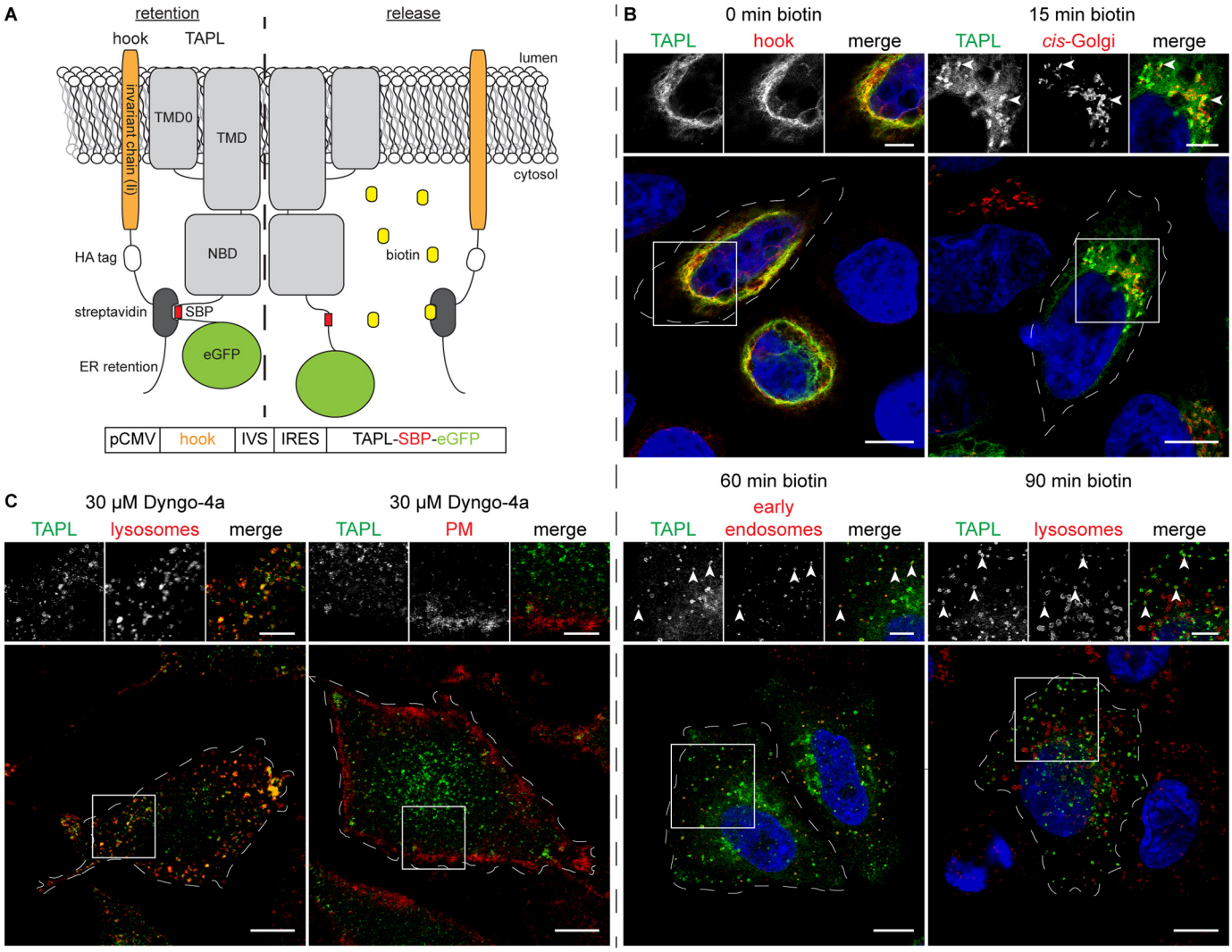

Figure 1. Intracellular route of TAPL. *A*, constructs for the RUSH assay. The invariant chain of MHC class II (luminal domain is not depicted), containing a cytosolic HA tag, streptavidin, and an ER retention signal, served as ER "hook" protein. TAPL was C-terminally fused to SBP and eGFP. To guarantee simultaneous expression, both genes were cloned in a bicistronic internal ribosome entry site (IRES) vector under the control of the cytomegalovirus promotor (*pCMV*) and separated by a synthetic intervening sequence (*IVS*) and an IRES. *B*, time-dependent trafficking of TAPL. HeLa Kyoto cells were transiently transfected with the bicistronic IRES vector coding for both RUSH constructs and incubated with biotin for the indicated times. Subsequently, cells were fixed and immunostained by α-HA (hook), α-GM130 (*cis*-Golgi), α-EEA1 (early endosomes), and α-LAMP-1 (late endosomes/lysosomes). *White arrowheads* at the *zoom-in* point to an overlap of TAPL and subcellular marker. *Scale bar*, 10 μm; *inset*, 5 μm. *C*, TAPL is not found on the plasma membrane. TAPL-FLAG expression was induced by doxycycline in stably transfected HeLa Flp-In T-REx cells in the presence of 30 μM Dyngo-4a for 2 h. Cells were fixed and immunostained by α-FLAG (TAPL) and α-LAMP-1 (lysosomes) or α-MHC I (plasma membrane). *Scale bars*, 10 μm and 5 μm (*inset*).

the cell population than would be possible in transiently transfected cells.

First, we replaced the conserved, positively charged residues with alanine and the conserved, negatively charged residues with asparagine. Asp-49 was always substituted in combination with Asp-45, which is one helical turn upstream of Asp-49 in TMH2 and could compensate for charge deletion of Asp-49. Subcellular localization was examined by confocal immunofluorescence microscopy (Fig. 3*A*), and lysosomal localization was quantified by Pearson correlation of 50 single cells (Fig. 3*B*). The substitution of any of the four conserved, charged residues interfered with trafficking of TAPL. $TAPL_{K100A}$ still displayed a substantial overlap with LAMP-1 (Pearson correlation coefficient (PCC) = 0.54 ± 0.02) but was significantly reduced compared with WT TAPL (PCC = 0.8 ± 0.1). Further reduction in lysosomal localization was detected for $TAPL_{D45N,D49N}$ (PCC = 0.24 ± 0.03) and $TAPL_{R57A}$ (PCC = 0.20 ± 0.02). Most strikingly, $TAPL_{D17N}$ was not detected in LAMP-1–positive compartments at all (PCC = −0.23 ± 0.03). $TAPL_{D17N}$ also showed no overlap with the *cis*-Golgi marker GM130 but strong colocalization with the ER marker protein disulfide-isomerase (Fig. S4). Because of this result, we replaced both conserved positive charged residues and observed that $TAPL_{R57A,K100A}$ (PCC = −0.19 ± 0.02) behaved like $TAPL_{D17N}$, showing no lysosomal localization. TAPL mutants, which are unable to reach lysosomes due to these substitutions, are localized in the ER. A pronounced ER localization could mask a weak lysosomal population in case of $TAPL_{D17N}$. Therefore, we treated the cells with cycloheximide (CHX) and chased them for 5 h to inhibit protein synthesis and allow trafficking (Fig. S5). Lysosomal localization of $TAPL_{D45N,D49N}$ (PCC = 0.27 ± 0.02) and $TAPL_{K100A}$ (PCC =

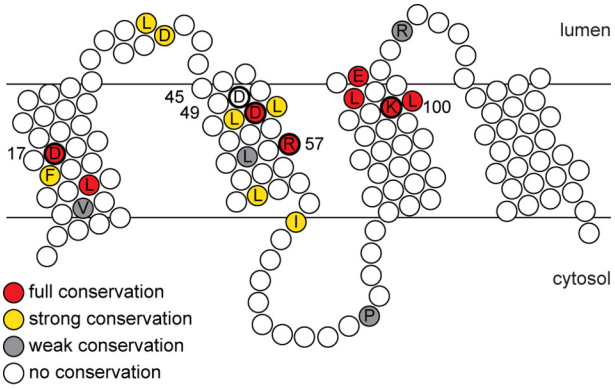

Figure 2. Conserved, charged residues within TMD0. Conserved residues of human, mouse, chicken, zebrafish, and sea lamprey TAPL, as well as *C. elegans* HAF-4 and HAF-9 (see Fig. S3), are depicted in a TMD0 secondary structure model (20). Charged residues within TMH1–3 investigated in this study are highlighted by a *boldface border*.

0.59 ± 0.02) was unaltered (Fig. S6). In contrast, lysosomal localization of $TAPL_{R57A}$ was significantly increased (PCC = 0.45 ± 0.02) by CHX treatment, implying a more challenging folding of $TAPL_{R57A}$. Importantly, $TAPL_{D17N}$ and $TAPL_{R57A,K100A}$ did not show colocalization with LAMP-1, confirming that these TAPL variants were unable to reach lysosomes and were stuck in the ER. In summary, substitution of the conserved, charged residues within TMD0 impacts lysosomal targeting of TAPL, and therefore these residues determine its subcellular localization. Moreover, TAPL was trapped in the ER if the positive charges at Arg-57 and Lys-100 or the negative charge at Asp-17 were deleted. Because the deletion of these charged residues had the same effect, we hypothesize that Asp-17 forms an intramolecular salt bridge with one of these two positively charged residues to yield a trafficking-competent conformation. It should be noted that the deletion of the positive charge at position 57 had a stronger effect than the charge removal at position 100.

If the ER localization of $TAPL_{D17N}$ was caused by disruption of a salt bridge, the simultaneous inversion of the charges of Asp-17 and Arg-57 or Lys-100 should yield a trafficking competent TAPL variant. To prove any lysosomal localization, we again applied CHX for 5 h (Fig. 4). $TAPL_{D17R}$ (PCC = −0.29 ± 0.02), like $TAPL_{D17N}$, showed no overlap with LAMP-1. $TAPL_{R57D}$ (PCC = −0.32 ± 0.02), in stark contrast to its neutral substitution $TAPL_{R57A}$, also fully lacked colocalization with LAMP-1, whereas $TAPL_{K100D}$ (PCC = 0.51 ± 0.02) was trafficked as well as $TAPL_{K100A}$ to lysosomes. These findings indicated that Arg-57 is more relevant for yielding a trafficking-competent conformation than Lys-100 and also possibly in closer proximity to Asp-17 for forming a salt bridge. This hypothesis was supported by the fact that $TAPL_{D17R,R57D}$ was indeed trafficking-competent and showed colocalization with lysosomes (PCC = 0.49 ± 0.02), strongly indicating a salt bridge between Asp-17 and Arg-57. In contrast, $TAPL_{D17R,K100D}$ (PCC = −0.27 ± 0.02) was not found in lysosomes, pointing to a minor role of Lys-100 in the context of Asp-17.

During the analysis of the conserved, charged residues in TMD0 of TAPL, we noticed that $TAPL_{D45N,D49N}$ showed a significantly reduced lysosomal localization compared with $TAPL_{wt}$ (Fig. 3). Inversion of the charges ($TAPL_{D45K,D49K}$ PCC = −0.27 ± 0.02) abolished lysosomal localization (Fig. 5, *A* and *B*). This effect could not be compensated by the additional substitution of K100D ($TAPL_{D45K,D49K,K100D}$ PCC = −0.16 ± 0.02). Whereas lysosomal localization was clearly absent, $TAPL_{D45K,D49K}$ and $TAPL_{D45K,D49K,K100D}$ showed strong colocalization with the *cis*-Golgi marker GM130 ($TAPL_{D45K,D49K}$ PCC = 0.50 ± 0.02 and $TAPL_{D45K,D49K,K100D}$ PCC = 0.56 ± 0.01) as detected in the presence (Fig. 5) as well as in the absence (Fig. S7) of CHX. Correct folding of the triple mutant $TAPL_{D45K,D49K,K100D}$ was demonstrated by similar peptide transport activity as $TAPL_{wt}$ (Fig. 5*C*). In conclusion, Asp-17 in TMH1 of TAPL and its salt bridge to Arg-57 are essential for the release of the transporter from the ER, whereas Asp-45 together with Asp-49 are important for the second trafficking step from the Golgi to the endosomal and lysosomal compartments.

$TAPL_{D17N}$ is correctly folded

Defects in trafficking and especially ER retention can be caused not only by missing trafficking determinants but also by misfolding. Therefore, we tested correct folding of $TMD0_{wt}$ and its mutants *in vivo* by the interaction with coreTAPL. We transiently co-expressed TMD0 variants containing a C-terminal FLAG tag and coreTAPL in HEK293T cells and performed co-immunoprecipitation with an α-FLAG antibody. CoreTAPL was precipitated together with all TMD0 variants but not in the absence of TMD0, demonstrating correct folding of all TMD0 mutants (Fig. 6*A*). Because substituting Asp-17 showed the strongest effects in subcellular trafficking and ER retention, we addressed the folding state of $TMD0_{D17N}$ and $TAPL_{D17N}$ in more detail. First, we evaluated folding of $TMD0_{D17N}$ by solution NMR. ^{15}N-Labeled variants of $TMD0_{wt}$ (cf-TMD0) and $TMD0_{D17N}$ (cf-$TMD0_{D17N}$) were synthesized by cell-free (cf) expression, and ^{15}N,^{1}H BEST-TROSY spectra were recorded (Fig. 6*B*). The well-resolved peak distribution and peak overlaps between both spectra indicated that cf-$TMD0_{D17N}$ is a folded protein with a conformation similar to cf-TMD0. Next, the localization of TMD0 in stably transfected HeLa Flp-In T-REx cells was analyzed (Fig. 6*C*). $TMD0_{wt}$ significantly overlapped with the lysosomal marker LAMP-1, whereas $TMD0_{D17N}$ was not localized in lysosomes. Adding the cytosolic, tyrosine-based lysosomal targeting sequence of LAMP-2C at the C terminus of $TMD0_{D17N}$ partially restored lysosomal localization (Fig. 6*D*). Therefore, ER retention must be due to the absence of a lysosomal targeting determinant in $TMD0_{D17N}$, whereas misfolding can be excluded. Lysosomal localization of full-length $TAPL_{D17N}$ was also recovered if co-expressed with $TAPL_{wt}$ in HeLa Kyoto cells, demonstrating that $TAPL_{D17N}$ dimerizes with $TAPL_{wt}$ and is not retained in the ER (Fig. 7, *A* and *B*). Finally, correct folding and dimerization of $TAPL_{D17N}$ was demonstrated by the comparable ATP-dependent peptide transport activity of $TAPL_{wt}$ and $TAPL_{D17N}$ in crude membranes derived from HeLa Flp-In T-REx cells (Fig. 7*C*). Taking these results together, we conclude that altered lysosomal trafficking and ER or Golgi retention of TAPL mutants are not caused by misfolding but are due to the absence of a targeting determinant.

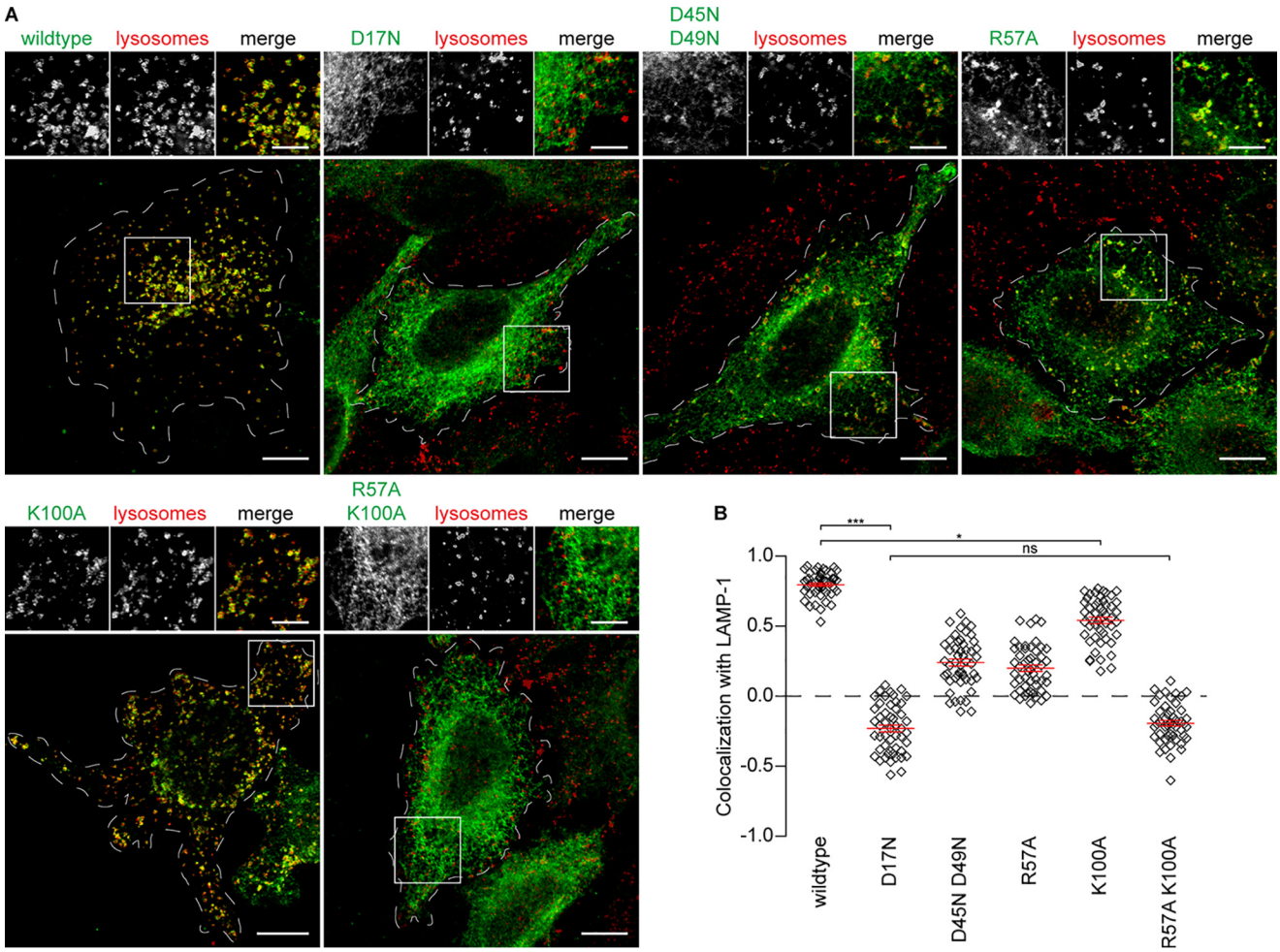

Figure 3. Conserved, charged residues within TMD0 determine TAPL localization. *A*, subcellular localization of TAPL mutants. 24 h after induction of TAPL variants expression, HeLa Flp-In T-REx cells were fixed and immunostained by α-FLAG (TAPL) and α-LAMP-1 (lysosomes). *Scale bar*, 10 μm; *inset*, 5 μm. *B*, quantification of lysosomal localization. For each TAPL construct, the Pearson correlation coefficient of TAPL and LAMP-1 colocalization was determined for 50 individual cells. Individual values are depicted as *rectangles*, and mean values and corresponding S.E. (*error bars*) are shown in *red*. ***, $p < 0.001$; *, $p < 0.05$; *ns*, nonsignificant by Kruskal–Wallis test with post hoc Dunn's test. Mean values, corresponding S.E., and test results are listed in Table S1.

Trafficking chaperones

Because the impaired ER to Golgi trafficking of $TAPL_{D17N}$ and $TAPL_{D17R}$ is not due to misfolding, we hypothesized that the identified salt bridge stabilizes a specific conformation of TMD0 that allows transient interactions with trafficking chaperones. The only known interaction partners for TAPL are LAMP-1 and -2B, identified by tandem affinity purification of digitonin-solubilized membranes. However, these proteins are negligible for TAPL trafficking, because in double LAMP-1/2 knockout cells, TAPL is correctly targeted to lysosomes (12). Therefore, we aimed to identify components of the trafficking interactome that are assumed to interact with TAPL only transiently and are consequently associated with TAPL in low abundance. Thus, we performed a fast, single-step purification followed by MS and applied Comparative Proteomic Analysis Suite (CompPASS) to enable identification of high-confidence candidate interacting proteins (HCIPs) (22). In short, CompPASS ranks identified proteins based on peptide abundance and occurrence in predetermined proteomic data sets. A protein frequently found across several samples in the data sets is ranked lower than a unique one in a given sample. HeLa Flp-In T-REx cells nontransfected or stably expressing TAPL-HA or coreTAPL-HA were solubilized by the detergent Nonidet P-40 (NP40), purified in a single step with an α-HA antibody, and analyzed by tandem MS. CompPASS analysis revealed 14 HCIPs of TAPL that were absent in coreTAPL samples or samples derived from untransfected cells. Among these HCIPs (Fig. 8*A*), the Yip1-interacting factor homologue B (YIF1B) is the only one that is a transmembrane protein and also involved in trafficking of a transmembrane protein. YIF1B is a member of the FinGER protein family and, together with YIF1A, the human homologues of yeast YPT-interacting protein 1 (YIP1). In prior studies, both proteins were implicated in ER-to-Golgi protein trafficking (23, 24). YIF1B is composed of an N-terminal cytosolic domain, followed by a C-terminal TMD composed of five predicted TMHs (Fig. S11*A*). First, we verified the interaction of TAPL with YIF1B by co-immunoprecipitation. Endogenous YIF1B was co-immunoprecipitated with C-terminally FLAG-tagged TAPL and TMD0 stably expressed in HeLa Flp-In T-REx cells, but not with coreTAPL (Fig. 8*B*). Importantly, TMD0 was pulled down in a reverse immunoprecipitation via YIF1B if transiently co-expressed in HEK293T cells

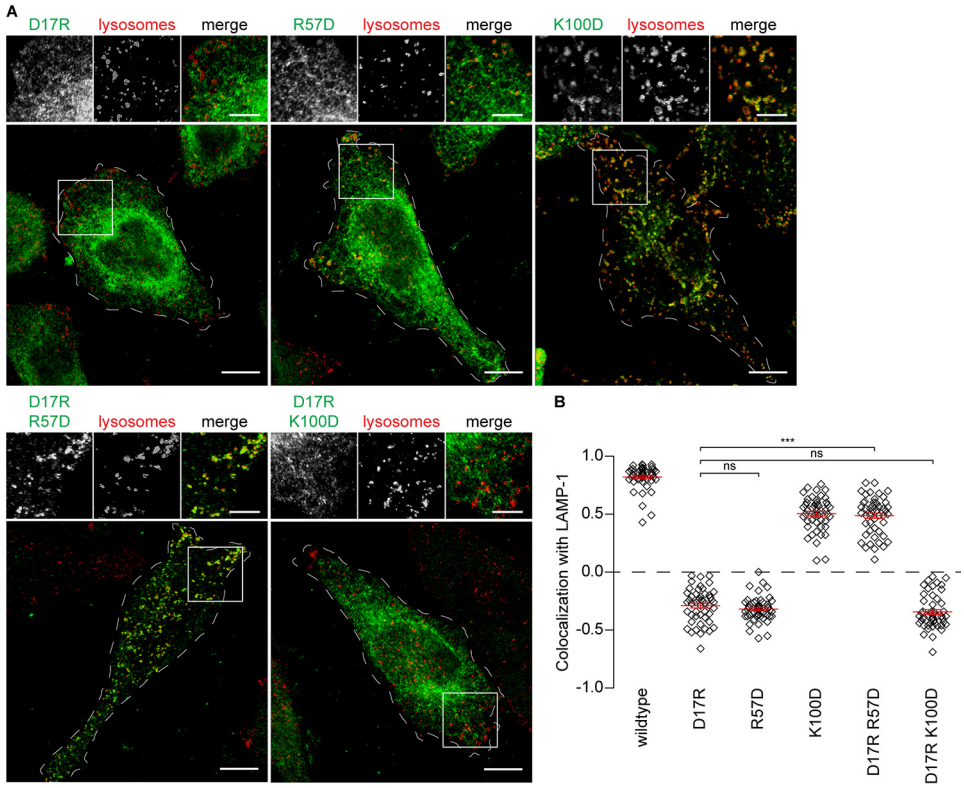

Figure 4. Intramolecular salt bridge between Asp-17 and Arg-57. *A*, subcellular localization of TAPL variants. 19 h after induction of TAPL variants expression, HeLa Flp-In T-REx cells were treated with 25 μg/ml CHX for 5 h. Cells were fixed and immunostained by α-FLAG (TAPL) and α-LAMP-1 (lysosomes). *Scale bars*, 10 μm and 5 μm (*insets*). *B*, quantification of lysosomal localization. For each TAPL construct, the Pearson correlation coefficient of TAPL and LAMP-1 colocalization was determined for 50 individual cells. Individual values are depicted as *rectangles*, and mean values and corresponding S.E. (*error bars*) are shown in *red*. ***, $p < 0.001$; *ns*, nonsignificant by Kruskal–Wallis test with post hoc Dunn's test. Mean values, corresponding S.E., and test results are listed in Table S1.

(Fig. 8*C*), demonstrating that YIF1B interacts with the TMD0 of TAPL. The TMD of YIF1B, devoid of its cytosolic tail, was still able to interact with TAPL in transiently co-transfected HEK293T cells (Fig. 8*D*), validating that the interaction occurs via the TMDs of both proteins.

Next, we investigated whether YIF1B is essential for TAPL targeting. HeLa Flp-In T-REx YIF1B knockout clones were created by CRISPR/Cas9 using two separate sgRNAs targeting exon 2 or exon 3. The knockout was confirmed by immunoblot and sequencing of the targeted exons (Fig. S8*A*). In the YIF1B knockout cell lines, TAPL showed no alteration in localization between 2 and 24 h after induction of expression compared with the original cell line (Figs. S8*B* and S9*A*). Next, YIF1B knockout cells were transfected with the aforementioned vector for the RUSH assay, yielding no differences in the early trafficking process of TAPL (Fig. S9*B*). This demonstrates that YIF1B is not essential for TAPL targeting and its absence does not impact trafficking kinetics. Redundancy in subcellular trafficking is common; therefore, we investigated whether YIF1A, with a sequence identity of 53% to YIF1B, can compensate for YIF1B deficiency (Fig. S10). Nevertheless, YIF1B, but not YIF1A, was co-immunoprecipitated with TMD0 if transiently co-expressed in HEK293T cells, consistent with the MS results.

To assess whether YIF1B plays a role in TAPL targeting, even if it is not an essential factor, we aimed to outcompete alternative binding partners as well as endogenous YIF1B by overexpression of truncated YIF1B (TMD_{YIF1B}). If we assume that YIF1B is involved in ER to Golgi targeting of TAPL and harbors its targeting determinant in its cytosolic domain, the overexpression of TMD_{YIF1B} should influence TAPL targeting. In contrast to YIF1B, which is found predominantly in the ER, TMD_{YIF1B} is strongly enriched in the *cis*-Golgi (Fig. S11, *B* and *C*), implying that a targeting or retrieval signal is indeed localized in the cytosolic domain of YIF1B. Upon transient co-expression in HeLa Kyoto cells, TAPL showed a reduction in lysosomal localization dependent on the TMD_{YIF1B} level (Fig. 9, *A*, *B*, and *E*), with more pronounced effects in cells with higher TMD_{YIF1B} levels. TAPL was strongly enriched in lysosomes of cells not transfected by YIF1B or TMD_{YIF1B}. Overexpression of TMD_{YIF1B} significantly decreased colocalization of TAPL with LAMP-1, compared with cells overexpressing full-length YIF1B (Fig. 9, *D* and *E*). Interestingly, TAPL colocalized strongly with TMD_{YIF1B} in *cis*-Golgi (Fig. 9*C*).

Finally, we tested our initial hypothesis that D17N substitution in TMD0 affects the interaction with YIF1B. HEK293T cells were transiently transfected with TMD0-FLAG or $TMD0_{D17N}$-FLAG, and immunoprecipitation was carried out using α-FLAG antibody. The amount of endogenous YIF1B pulled down by $TMD0_{D17N}$ was reduced by a factor of 4 compared with TMD0 (Fig. 9, *F* and *G*), based on the four individual immunoprecipitations we performed (Fig. S12). This indicates a conformational change of the TMD0 interaction interface by disruption of the salt bridge between Asp-17 and Arg-57.

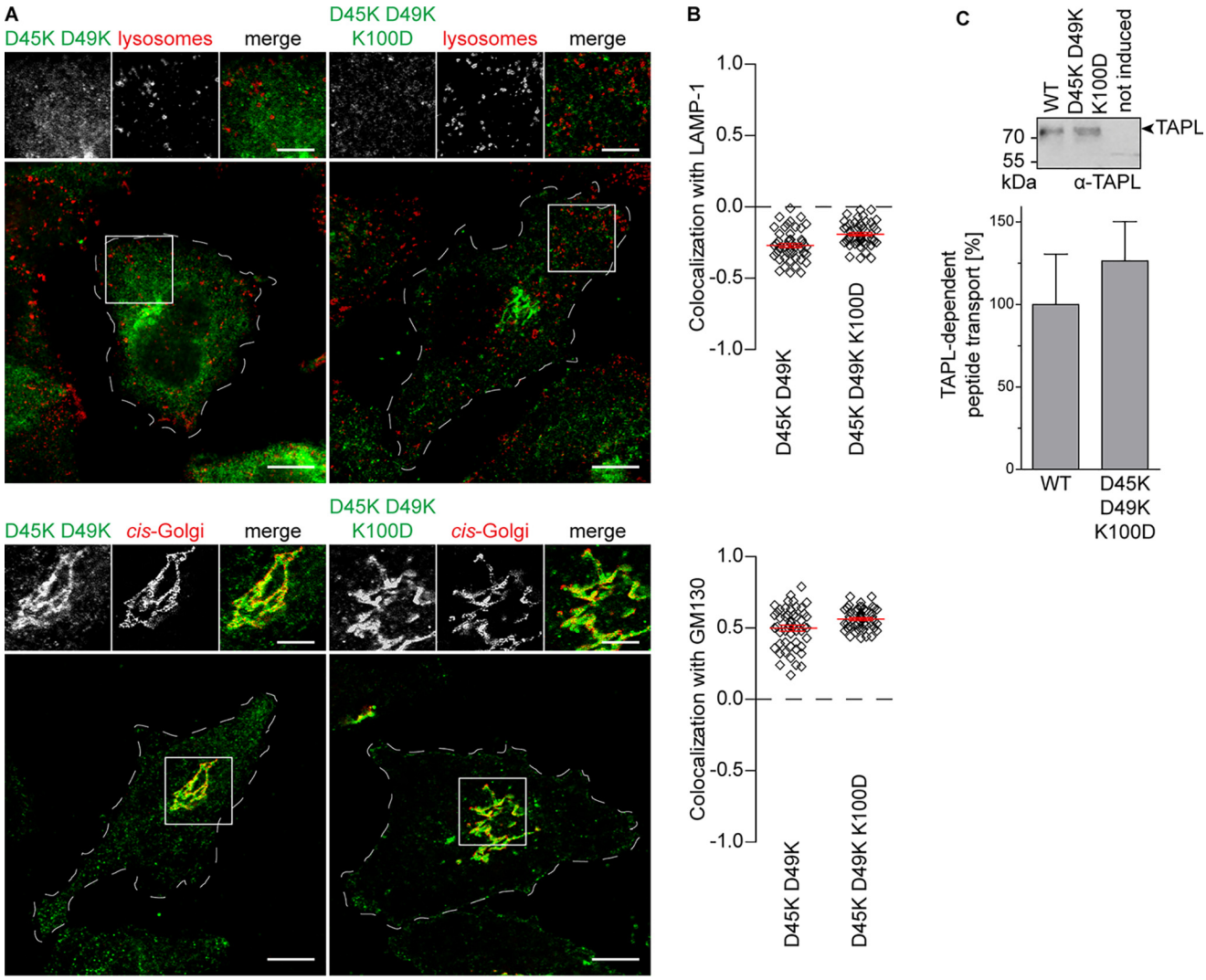

Figure 5. Golgi retention of TAPL substitutions. *A*, subcellular localization of TAPL variants. 19 h after induction of TAPL variant expression, cells were treated with 25 μg/ml CHX for 5 h. Cells were fixed and immunostained by α-FLAG (TAPL), α-LAMP-1 (lysosomes), or α-GM130 (*cis*-Golgi). *Scale bars*, 10 μm and 5 μm (*insets*). *B*, quantification of subcellular localization. For each TAPL construct, the Pearson correlation coefficient of TAPL and LAMP-1 or GM130 colocalization was determined for 50 individual cells. Individual values are depicted as *rectangles*, and mean values and corresponding S.E. (*error bars*) are shown in *red*. *C*, TAPL substitutions are correctly folded. Peptide transport of crude membranes derived from HeLa Flp-In T-REx cells not transfected or containing TAPL constructs was performed with NST-F peptide (3 μM) in the presence of ATP (3 mM) for 12 min at 37 °C. Peptide accumulation in crude membranes from not transfected cells was subtracted. Transport, performed in triplicates, was normalized to TAPL amount determined by immunoblot of crude membranes derived from HeLa Flp-In T-REx cells not induced (5 μg) or expressing WT TAPL (2.5 μg) or $TAPL_{D45K,D49K,K100D}$ (5 μg). *Error bars*, S.D.

In summary, the newly identified transient interaction partner YIF1B interacts via its TMD_{YIF1B} directly or indirectly with TMD0. Although YIF1B is not essential for lysosomal targeting of TAPL, overexpression of TMD_{YIF1B} strongly interferes with the correct localization of TAPL. Interaction of both proteins is strongly dependent on the conserved Asp-17 within TMD0.

Discussion

In this study, we demonstrated that TAPL takes the direct route from the Golgi to lysosomes. Further, we found four conserved, charged amino acids in the transmembrane helices of TMD0, which affect the subcellular localization of TAPL and, therefore, represent atypical targeting determinants. Additionally, we identified YIF1B as a new interaction partner of TAPL, being the first piece of the, presumably more complex, trafficking interactome.

By synchronizing intracellular trafficking using the RUSH assay, we proved that TAPL chooses the direct route to lysosomes via the Golgi and early endosomes but not the indirect route via the PM. The lack of PM localization is supported by the use of the dynamin inhibitor Dyngo-4a and missing surface biotinylation (11). Furthermore, TAPL was not detected on the PM in bone marrow-derived dendritic cells (8). This is in contrast to lysosome-localized ABCB6, which takes the indirect route and can be accumulated at the PM by adding Dyngo-4a (25). Although the trafficking kinetics should be analyzed with caution due to their dependence on cells with high TAPL-SBP-eGFP levels for detection, rough estimates can be made based on our results. ER-to-Golgi trafficking occurs within 15–30 min after the addition of biotin. After 30 – 60 min, Golgi localization decreases, and early endosome localization is detectable. To reach lysosomes, TAPL needs up to 90 min. This time frame is

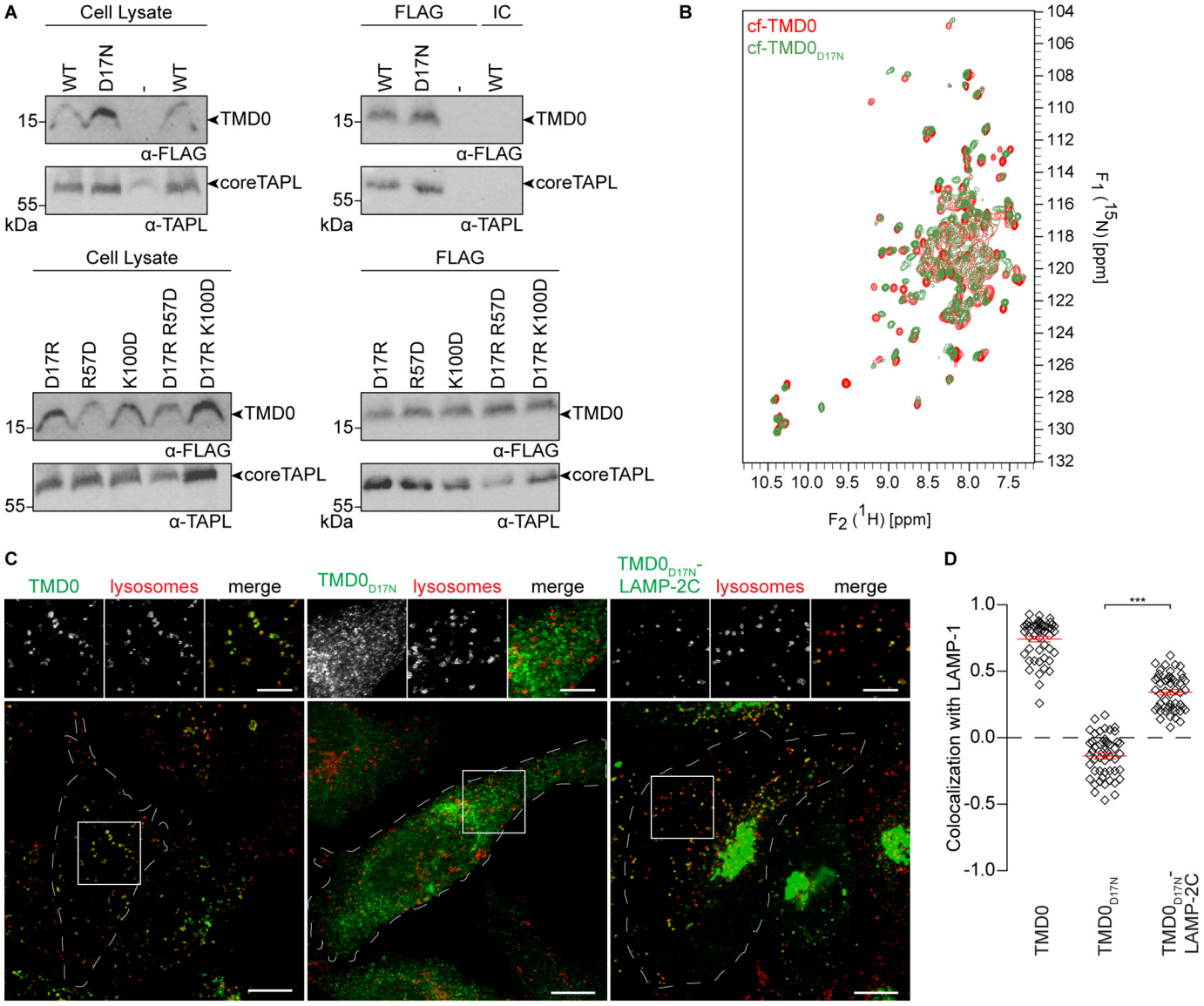

Figure 6. TMD0 is correctly folded. *A*, TMD0 variants interact with coreTAPL. HEK293T cells transiently co-transfected with TMD0-FLAG constructs and coreTAPL were solubilized by 1% digitonin (cell lysate). Co-immunoprecipitation was performed using α-FLAG antibody (FLAG) or an IgG isotype control antibody (*IC*). CoreTAPL was detected by α-TAPL. *B*, structural integrity of $TMD0_{D17N}$. ^{15}N,^{1}H BEST-TROSY NMR spectra were recorded of ^{15}N-uniformly labeled cf-TMD0 (*red*) and cf-$TMD0_{D17N}$ (*green*) at 313 K. *C*, restoration of lysosomal localization of $TMD0_{D17N}$. 24–48 h after induction of TMD0-FLAG, FLAG-$TMD0_{D17N}$, and FLAG-$TMD0_{D17N}$-LAMP-2C expression, HeLa Flp-In T-REx cells were fixed and immunostained by α-FLAG for TMD0 constructs and α-LAMP-1 (lysosomes). *Scale bars*, 10 μm and 5 μm (*insets*). *D*, quantification of lysosomal localization. For each TMD0 construct, the Pearson correlation coefficient of TMD0 and LAMP-1 colocalization was determined for 50 individual cells. Individual values are depicted as *rectangles*, and mean values and corresponding S.E. (*error bars*) are shown in *red*. ***, $p < 0.001$ by Kruskal–Wallis test with *post hoc* Dunn's test. Mean values, corresponding S.E., and additional test results are listed in Table S1.

in line with data from inducible HeLa Flp-In T-REx cells used in this study, where TAPL co-localized with LAMP-1 2 h after induction of expression. Moreover, the trafficking time of TAPL is in good agreement with that of other proteins in the secretory pathway and lysosomal membrane proteins (26–28).

Atypical cytosolic targeting determinants, which differ from the consensus tyrosine or dileucine motifs, can be found, for example, in the Longin domain of VAMP7 (29) as PY motifs ((L/P)PXY) in LAPTM5 (30) or as "extended acidic dileucine signal" in TMEM106B (31). For some proteins, these motifs are, by themselves, not sufficient to mediate lysosomal localization but are dependent on additional motifs. One example is the lysosomal targeting of TMEM106B, which additionally depends on *N*-glycosylation of its luminal loops (32). Another type of atypical sorting determinants is TMH parameters like their length, amount, and positioning of hydrophobic or charged amino acids or interplay with lipids (33). In the case of TAPL, charged amino acids within the TMHs of TMD0 determine its subcellular localization. Charged residues within TMHs are often essential for protein function and complex assembly. For instance, correct complex assembly and therefore PM localization of the T-cell receptor depends on charged residues in the TMHs (34, 35). In the case of $TAPL_{D17N}$, full ER retention is not due to an incomplete assembly of TAPL homodimers because $TAPL_{D17N}$ is fully active in peptide transport. By means of immunoprecipitations, NMR analysis of

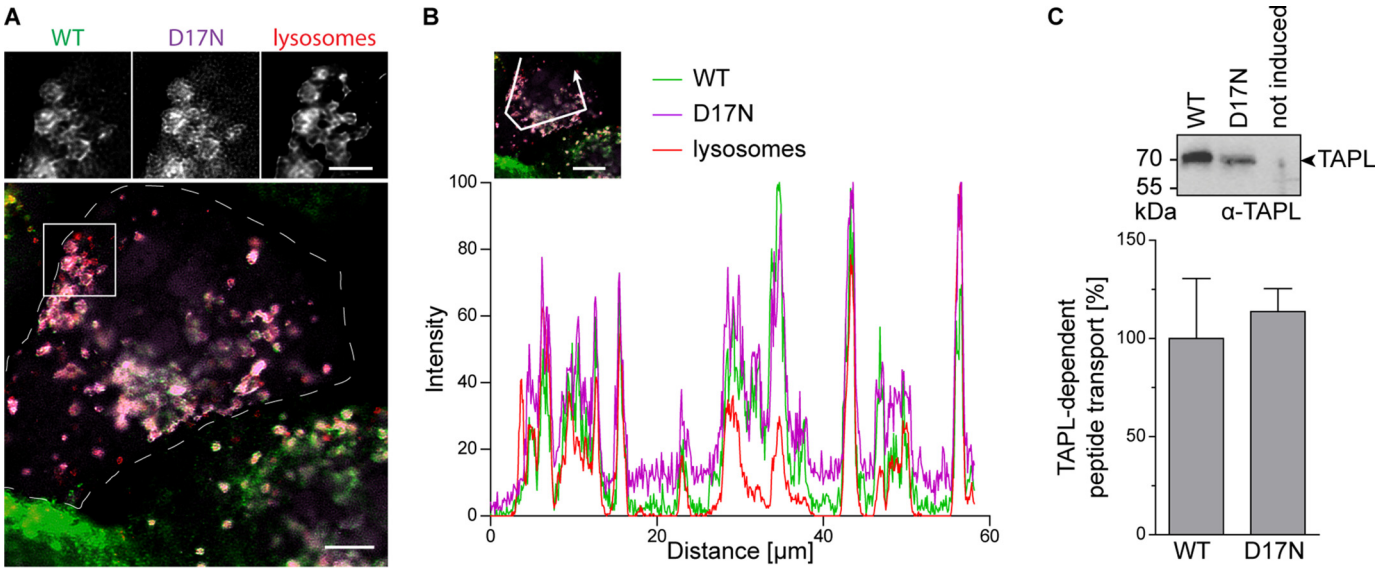

Figure 7. $TAPL_{D17N}$ is correctly folded. *A*, $TAPL_{D17N}$ is accompanied to lysosomes by $TAPL_{wt}$. HeLa Kyoto cells, transiently co-transfected with TAPL-FLAG and $TAPL_{D17N}$-C8, were fixed and stained by α-C8, α-FLAG, and α-LAMP-1 (lysosomes). *Scale bars*, 5 μm and 2.5 μm (*insets*). *B*, $TAPL_{D17N}$, $TAPL_{wt}$, and LAMP-1 colocalize. Intensity of all three channels from the micrograph depicted in *A* is shown along the *white arrow* for better visualization. *Scale bar*, 10 μm. *C*, TAPL-dependent peptide transport. Peptide transport of crude membranes derived from HeLa Flp-In T-REx cells not transfected or containing $TAPL_{wt}$ or $TAPL_{D17N}$ was performed with NST-F peptide (3 μM) in the presence of ATP (3 mM) for 12 min at 37 °C. Peptide accumulation in crude membranes from untransfected cells was subtracted. Transport, performed in triplicates, was normalized to TAPL amount determined by immunoblotting of crude membranes derived from HeLa cells not induced (5 μg) or expressing WT TAPL (2.5 μg) or $TAPL_{D17N}$ (10 μg). TAPL WT data are taken from Fig. 5*C* because the experiments were performed for all mutants simultaneously. *Error bars*, S.D.

cf-$TMD0_{D17N}$, and restoration of lysosomal localization of $TMD0_{D17N}$ by supplying the targeting motif of LAMP-2C, we demonstrated that ER retention was also not caused by misfolding. In conclusion, whereas Asp-17 is indispensable for targeting, it is not essential for the structural integrity of TAPL or TMD0.

YIF1B shuttles between ER, ERGIC, and Golgi (23). Furthermore, it is involved in lysosomal trafficking of TAPL, because overexpression of TMD_{YIF1B}, which accumulates in the Golgi, has a strong impact on TAPL targeting. Moreover, TMD0 of TAPL interacts transiently with TMD_{YIF1B}, and this interaction is strongly weakened by mutating Asp-17 of TAPL. Therefore, we postulate that subcellular targeting of TAPL depends on its interactions with other transmembrane proteins that link it to components of the trafficking machinery. Because YIF1B is not implicated in trafficking steps beyond the Golgi, other transmembrane proteins probably interact with TAPL at the TGN and endosomes to mediate further trafficking steps. This would coincide with the observed strong Golgi retention of TAPL upon Asp-45, Asp-49, and Lys-100 substitution. Such a piggyback mechanism is described for the ABC transporter ABCD4, which interacts with the classical tyrosine-based motif exhibiting LMBD1 (36). Similarly, the endosomal and lysosomal localization of MHC class II is the result of its interaction with the invariant chain (37, 38), which blocks premature peptide binding (39) and also exhibits a dileucine motif (40).

YIF1B, implicated in anterograde transport (23), plays a role in 5-HT_{1A} receptor trafficking (41). However, this cell surface–localized protein interacts with YIF1B via its cytosolic tail and not its TMD. In contrast, the closely related YIF1A, which shares high sequence identity in its TMD with YIF1B, interacts with VAPB via its transmembrane domain (24), indicating that these proteins may have multiple binding sites for different proteins. Despite their similarities in the TMD, YIF1A is unable to interact with TMD0, as demonstrated by immunoprecipitation.

CRISPR/Cas9-mediated knockout of YIF1B in our stable cell line system did not alter TAPL localization and is therefore apparently not an essential factor for targeting. Thus, other transmembrane proteins also have to be considered for TAPL ER to Golgi trafficking. Redundant trafficking pathways and mechanisms are observed for several proteins. For instance, three different trafficking routes were described for LAMP-1/2. Usually, these proteins are trafficked in a clathrin-dependent manner. They can either take the direct route (42), mediated by AP-1 (43) and AP-3 (44), or the indirect route, mediated by AP-2 (45). Additionally, trafficking from the TGN to late endosomes by non-clathrin-coated "LAMP carriers" was described (46, 47).

Of the four conserved charged residues, Asp-17 substitutions revealed the strongest impact on TAPL localization. Mutation of Asp-17 retained TAPL completely in the ER, whereas single substitutions of the other conserved amino acids allowed partial lysosomal localization. Intriguingly, the other two members of the TAP family, TAP1 and TAP2, which form heterodimers, also have a conserved aspartate in their first and a conserved arginine in their second TMH (48). It was shown that this aspartate is essential for an intermolecular salt bridge with tapasin. This interaction is placing TAP in the peptide loading complex, which is responsible for MHC class I loading. Based on molecular dynamics simulations, this aspartate forms an intramolecular salt bridge with the arginine, which is replaced by an intermolecular salt bridge with Lys-428 in the transmembrane helix of tapasin, whereas the arginine side chain snorkels to the polar headgroups of the lipid bilayer to avoid an unfavorable uncompensated charge in the TMD. Based on the strong

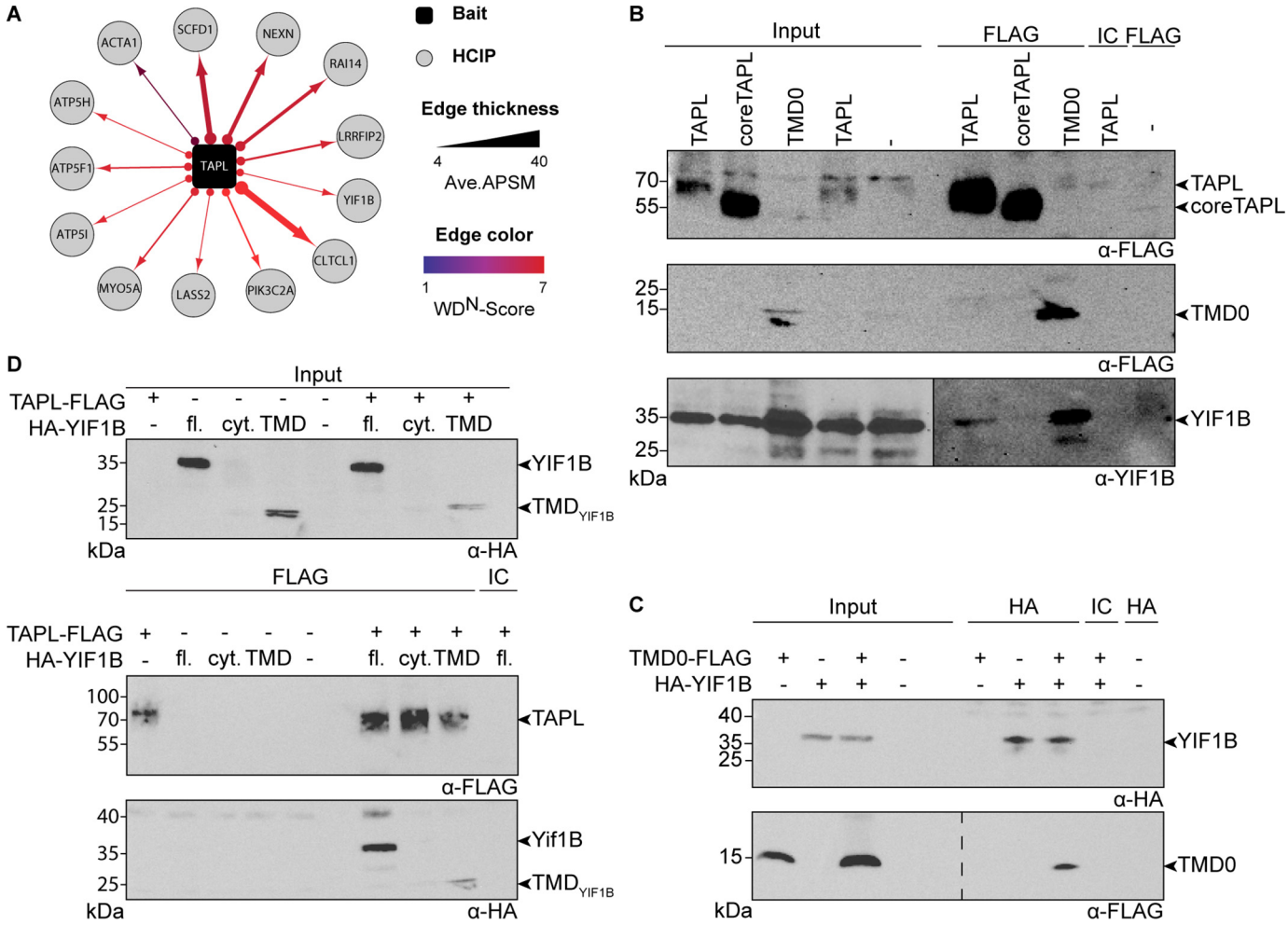

Figure 8. YIF1B interacts with TAPL. *A*, TMD0-dependent TAPL interactome. HeLa Flp-In T-REx cells stably expressing HA-tagged $TAPL_{wt}$ or coreTAPL and their parental empty counterparts were lysed by NP40 and subjected to IP-MS. HCIPs were identified by CompPASS based on a WD^N score ≥ 1.0 and APSM value ≥ 4. Proteins found in coreTAPL or parental nontransfected HeLa Flp-In T-Rex were subtracted from the TAPL HCIPs. *B*, YIF1B interacts with TAPL via TMD0. HeLa Flp-In T-REx cells stably expressing FLAG-tagged variants of $TAPL_{wt}$, coreTAPL or $TMD0_{wt}$ were solubilized by NP40, immunoprecipitated by α-FLAG antibody (*FLAG*), and immunoblotted. Specificity of immunoprecipitation was verified by an IgG isotype control (*IC*) and using nontransfected cells. The contrast in the *right part* of α-YIF1B immunoblot was enhanced due to low signal intensity. *C*, reverse co-immunoprecipitation of YIF1B and TMD0. HEK293T cells transiently transfected with $TMD0_{wt}$-FLAG, HA-YIF1B, or a combination of both were lysed by NP40. YIF1B was immunoprecipitated by α-HA antibody (*HA*) and immunoblotted. Specificity of immunoprecipitation was verified by an IgG isotype control and using cells transfected with a plasmid devoid of a gene of interest (−/−). *D*, TMD_{YIF1B} interacts with TAPL. HEK293T cells transiently transfected with $TAPL_{wt}$-FLAG alone or in combination with HA-YIF1B (*fl.*), HA-cyt_{YIF1B} (*cyt.*), or HA-TMD_{YIF1B} (*TMD*) were solubilized by NP40, and immunoprecipitation was performed by α-FLAG antibody. Specificity of immunoprecipitation was verified by an IgG isotype control and using cells transfected with a plasmid devoid of a gene of interest (−/−).

impact of charge inversion substitutions of Asp-17 and Arg-57 on TAPL trafficking, as well as the partial rescue of lysosomal localization by simultaneous charge reversal of both, we demonstrated that Asp-17 in TAPL does not form an intermolecular salt bridge but an intramolecular one with Arg-57. However, deletion of the charge at Arg-57 was partially compensated by Lys-100 because R57A substitution, unlike D17N, did not abolish lysosomal localization. This indicates that Asp-17 and Lys-100 are able to form a salt bridge but yield a conformation that is less trafficking-competent than the WT conformation. Charge inversion of Asp-17 and Lys-100 ($TAPL_{D17R,K100D}$) does not produce a trafficking-competent conformation, possibly due to the positive charge of Arg-57, which would be in close proximity to D17R, causing destabilizing effects. In line with the proposed salt bridges, deletion of both conserved positive charges again completely prohibited lysosomal targeting. Summing up our data, we propose that disruption of the salt bridge between Asp-17 and Arg-57 induces subtle conformational changes in the binding interface. These changes weaken the interaction with YIF1B and possibly other trafficking chaperones, resulting in increased ER localization of TAPL.

Interestingly, substitution and charge reversals of Asp-45, Asp-49, and Lys-100 strongly increased Golgi localization and also abolished lysosomal localization, further highlighting the importance of the conserved, charged residues. Whether a salt bridge is formed between Lys-100 and the negative cluster of Asp-45/Asp-49 cannot be derived from these experiments. These substitutions seem to impact the second trafficking step of TAPL from the Golgi to early endosomes, indicating an involvement in a second protein interaction interface, separate from that affected by Asp-17 and Arg-57 substitutions.

In summary, TAPL targeting is determined by conserved, charged residues in its TMD0, forming intramolecular salt bridges. Disruption of these salt bridges arrests TAPL either in

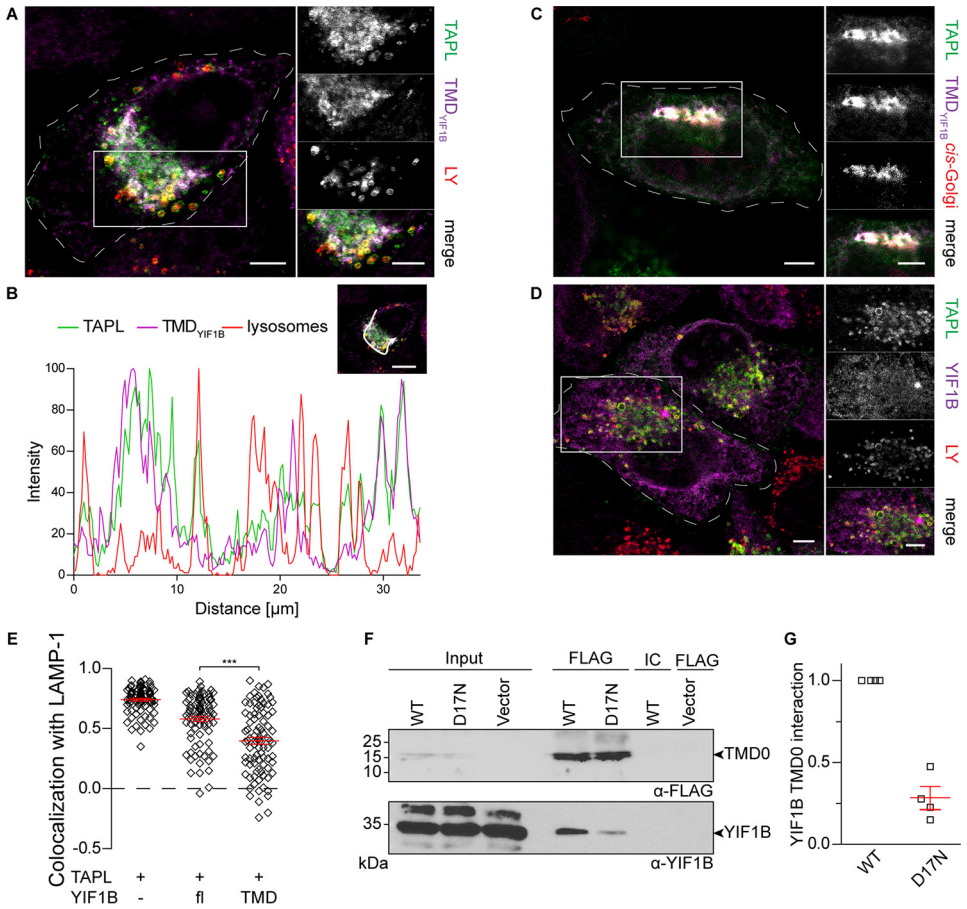

Figure 9. YIF1B is involved in TAPL targeting, and its interaction is weakened by D17N substitution. *A*, TMD of YIF1B interferes with TAPL targeting. HeLa Kyoto cells were transiently co-transfected with TAPL$_{wt}$-FLAG and HA-TMD$_{YIF1B}$. After 24 h, cells were fixed and stained by α-HA (TMD$_{YIF1B}$), α-FLAG (TAPL), and α-LAMP-1 (lysosomes/LY). *Scale bar*, 5 μm; *inset*, 5 μm. *B*, intensity of all three channels of micrograph depicted in Fig. 9*A* is shown along the *white arrow* for better visualization of colocalization. *Scale bar*, 10 μm. *C*, TMD$_{YIF1B}$ accumulates TAPL in the Golgi. HeLa Kyoto cells were transiently co-transfected with TAPL$_{wt}$-FLAG and HA-TMD$_{YIF1B}$. After 24 h, cells were fixed and stained by α-HA, α-FLAG, and α-GM130 (*cis*-Golgi). *Scale bar*, 5 μm; *inset*, 5 μm. *D*, TAPL is localized in lysosomes if full-length YIF1B is coexpressed. HeLa Kyoto cells were transiently co-transfected with TAPL$_{wt}$-FLAG and HA-YIF1B. After 24 h, cells were fixed and stained by α-HA (TMD$_{YIF1B}$), α-FLAG (TAPL), and α-LAMP-1 (lysosomes/LY). *All scale bars*, 5 μm. *E*, for quantification of YIF1B-dependent lysosomal localization of TAPL by Pearson correlation coefficient, 90 individual cells were quantified for each transfection. Individual values are depicted as *rectangles*, and mean values and corresponding S.E. (*error bars*) are shown in *red*. ***, $p < 0.001$ by Kruskal–Wallis test with post hoc Dunn's test. Mean values, corresponding S.E., and additional test results are listed in Table S1. *F*, Asp-17 of TAPL is important for YIF1B interaction. HEK293T cells transiently transfected with TMD0$_{wt}$-FLAG or TMD0$_{D17N}$-FLAG were lysed by NP40. TMD0 variants were immunoprecipitated by α-FLAG antibody (*FLAG*) and immunoblotted using α-FLAG and α-YIF1B. Specificity of immunoprecipitation was verified by an IgG isotype control (*IC*) and using cells transfected with a plasmid devoid of a gene of interest (*Vector*). *G*, YIF1B and TMD0-FLAG immunoblot signals from four independent experiments were quantified, and the TMD0$_{wt}$-FLAG-normalized ratio of YIF1B to TMD0 is plotted. Individual immunoblots used for quantification are shown in Fig. S12. Individual data points are shown as *squares*, and mean value and corresponding S.D. (*error bars*) are depicted in *red*.

the ER or Golgi by rendering TMD0 trafficking-incompetent. This inability to travel along the direct route to lysosomes is due to a diminished capability to interact with interaction partners involved in trafficking as exemplified with YIF1B.

Experimental procedures

Peptides and antibodies

Primary and secondary antibodies used in this study are listed in Table S2. α-YIF1B was a kind gift from Michèle Darmon (Centre de Psychiatrie et Neuroscience, Paris, France) (41). α-C8 was obtained through the AIDS Research and Reference Reagent Program, Division of AIDS, NIAID, National Institutes of Health: Chessie 8 from Dr. George Lewis (49). HA peptide was purchased from Sigma-Aldrich/Merck and Charité (Berlin, Germany). RRYQNSTCL peptide (Charité) was labeled with 5-iodoactamidofluorescein (I9271; Sigma-Aldrich/Merck) as described elsewhere (50).

Cloning

Cloning primers, corresponding templates, plasmids, and cloning techniques are listed in Table S3. The Q5 site-directed mutagenesis kit (New England Biolabs) was used according to the manufacturer's instructions. Restriction enzyme cloning was performed by digesting backbone and PCR product with the listed restriction enzymes (Thermo Fisher Scientific or New England Biolabs). Str-Ii_VSVGwt-SBP-EGFP (16) was a gift from Franck Perez (Institute Curie, Paris, France), and pSpCas9(BB)-2A-Puro (PX459) version 2.0 was a gift from Feng Zhang (Addgene plasmid 62988) (51). HA-YIF1A and HA-YIF1B genes were synthesized by Eurofins Genomics. All constructs were verified by DNA sequencing.

DNA extraction

To extract DNA from mammalian cells for PCR, 0.1×10^6 cells were transferred in a tube, washed three times with PBS

(4.3 mM Na_2HPO_4, 1.47 mM KH_2PO_4, 137 mM NaCl, 2.7 mM KCl, pH 7.4), and frozen at −20 °C. Pellet was resuspended in TE buffer (10 mM Tris-HCl, 1 mM EDTA, pH 8.0), incubated at 80 °C for 10 min, and then incubated at −20 °C for 5 min. Proteinase K (0.5 μg/μl, Thermo Fisher Scientific) was added and incubated at 50 °C for 30 min and at 80 °C for 10 min. Samples were centrifuged at 10,000 × *g* for 2 min, and 1 μl of supernatant was used as template for PCR.

Cell culture

HeLa Kyoto, HEK293T, and HeLa Flp-In T-REx cells were cultured at 37 °C, 5% CO_2, and 95% humidity. HeLa Kyoto and HEK293T were cultured in Dulbecco's modified Eagle's medium (DMEM) (Gibco/Thermo Fisher Scientific) with 10% fetal calf serum (FCS; Capricorn Scientific). For culturing stable cell lines of the HeLa Flp-In T-REx system, DMEM with 10% tetracycline-free FCS (Bio&Sell) was used. Selection of stable HeLa Flp-In T-REx cells was performed with 200 μg/ml hygromycin B (Thermo Fisher Scientific) in combination with 2 μg/ml blasticidin S HCl (Thermo Fisher Scientific). Selection of transiently transfected HeLa Flp-In T-REx cells was performed with 1 μg/ml puromycin (Thermo Fisher Scientific). Induction of expression in stable HeLa Flp-In T-REx cells was performed with 1 ng/ml to 5 μg/ml doxycycline (D9891; Sigma-Aldrich/Merck), depending on the gene of interest and application. For CHX (2112, Cell Signaling Technology) treatment, cells were induced for 19 h and then treated with 25 μg/ml CHX for an additional 5 h. All cells were tested regularly for mycoplasma contamination.

Transfection

Transfections of HeLa Kyoto, HeLa Flp-In T-REx, and HEK293T Flp-In T-REx cells were performed with Lipofectamine 2000 (Thermo Fisher Scientific) in a 1:2.5 ratio (μg of DNA/μl of transfection reagent). HEK293T cells were transfected using 18 mM polyethyleneimine (PEI) stock solution in a 1:5 ratio (μg of DNA/μl of transfection reagent). We used 0.8 μg of DNA/well in a 24-well plate, 2.5 μg DNA/well in a 6-well plate, and 15 μg for 10-cm dishes. DNA and Lipofectamine 2000 or PEI were diluted in Opti-MEM I medium (Thermo Fisher Scientific), incubated for 5 min, mixed, and incubated for 15 min prior to transfection. Cells were seeded 6–20 h prior to transfection to ensure complete adhesion. Lipofectamine 2000 and PEI transfections were performed at 80–95 and 40% confluence, respectively.

CRISPR/Cas9

Exon and intron sequences were obtained from the Ensembl Genome Browser (http://www.ensembl.org).[3] Exon 2 or 3 was used as an input sequence for sgRNA design. sgRNAs were picked according to their score and potential off-target effects (Table S3). Corresponding DNA was ordered from Eurofins Genomics. SpCas9–2A-Puro version 2.0 was used for transfection of HeLa-Flp-In T-REx cells. Selection was performed using puromycin. Post-selection limited dilution cloning was performed to obtain monoclonal cells. DNA was extracted and used for PCR. PCR products were separated by 2% agarose gel, extracted, purified, and sequenced. Knockout was further confirmed by immunoblot (52, 53).

Sequence alignments

All protein sequences were obtained from UniProt (http://www.uniprot.org)[3] (54). Sequence alignments were performed as Multiple Sequence Comparison by the Log-Expectation (MUSCLE) online tool (http://www.ebi.ac.uk/Tools/msa/muscle)[3] (55, 56).

Immunostaining

Cells were seeded on sterile coverslips in 24-well plates, washed three times with PBS, and fixed using 4% formaldehyde (Carl Roth) in PBS for 10 min. Permeabilization and blocking were performed by the addition of 0.1% saponin (S4521, Sigma-Aldrich/Merck) in PBS for 20 min and 5% BSA (Carl Roth) in 0.1% saponin/PBS, respectively. Cells were stained by primary and secondary antibody, diluted in 0.1% saponin/PBS containing 1% BSA, at room temperature for 2 and 1 h, respectively. 4′,6-Diamidino-2-phenylindole dihydrochloride (D8417, Sigma-Aldrich/Merck) was added during incubation with secondary antibody. After washing and drying, coverslips were mounted in Mowiol 4-88 and DABCO (Carl Roth).

Confocal imaging

The intracellular route of TAPL was imaged using a confocal laser-scanning TCS SP5 microscope (Leica) with a plan-apochromat ×63/1.4 oil differential interference-contrast objective. Sequential settings for scans were used. For excitation, the following laser lines were used: 405 nm (diode laser) for 4′,6-diamidino-2-phenylindole, 488 nm (argon laser) for eGFP, 561 nm (diode-pumped solid-state laser) for Cy3, and 633 nm (helium-neon laser) for Alexa Fluor 647. Intensities of channels were adjusted over the whole image for better visualization of overlap and exported by Leica Application Suite X.

All other experiments were performed using a confocal laser-scanning LSM880 microscope (Zeiss) with a plan-apochromat ×63/1.4 oil differential interference-contrast M27 objective. Sequential settings for scans were used. For excitation, the following laser lines were used: 488 nm (argon laser) for Alexa Fluor 488 and eGFP, 543 nm (helium-neon laser) for Cy3, 594 nm (helium-neon laser) for Alexa Fluor 568, and 633 nm (helium-neon laser) for Alexa Fluor 647. Intensities of channels were adjusted over the whole image for better visualization of overlap and exported by Zen blue (version 2.3 lite, Zeiss).

Live-cell imaging

Cells were cultured and transfected in 8-well x-well slides (Sarstedt). 18–24 h after transfection, cells were washed once with PBS and then shortly incubated in 200 μl of live-cell imaging solution (Invitrogen/Thermo Fisher Scientific) in the incubation chamber of the microscope at 37 °C. 200 μl of biotin (80 μM) in live-cell imaging solution was added to release TAPL-SBP-eGFP. *z*-stacks were recorded every 60–90 s. Maximum intensity *z*-projections were generated using Zen black (version 2.3, Zeiss).

[3] Please note that the JBC is not responsible for the long-term archiving and maintenance of this site or any other third party hosted site.

Quantification of colocalization

Unprocessed micrographs were exported by ZEN blue as .tiff files without compression. Images were loaded into Fiji/ImageJ (57, 58). Then 50–90 individual cells were outlined as regions of interest, and the PCC was determined by Coloc 2. Automated threshold selection (Costes) was performed. PCC values above threshold were plotted by GraphPad Prism version 5 (GraphPad Software) as a vertical scatter plot with means and S.E. $p < 0.05$ was considered significant. For intensity plots, intensity along the line was measured by Zen blue, normalized, and plotted by GraphPad Prism 5.

Statistical analysis

Statistical significance analyses were performed using GraphPad Prism 5 (GraphPad Software). For pairwise comparison statistics, unpaired two-tailed Student's *t* tests were applied. For multiple comparison of flow cytometry data, one-way analysis of variance with post hoc Tukey's test was used. For multiple comparisons of PCC values obtained from colocalization analysis, the nonparametric Kruskal–Wallis test with post hoc Dunn's test was used. Test results are listed in Table S1.

Deconvolution of images

All microscopy images, except maximum intensity *z*-projections, used for the figures were deconvoluted. Point-spread functions (PSFs) were generated by PSF Generator (59) for Fiji/ImageJ, using the Born–Wolf algorithm. Images were deconvoluted using DeconvolutionLab2 (60) for Fiji/Image2, using the Richardson–Lucy algorithm with 50 iterations.

Synthesis of Dyngo compounds

Dyngo-4a and Dyngo-Ø were synthesized as described recently (61) using the reflux method. Products were dissolved as 30 mM stock solutions in 100% DMSO (D2650, Sigma-Aldrich/Merck) and stored at −20 °C. Compounds were diluted in DMEM without FCS to 30 μM directly before usage.

Transferrin uptake assay

Transferrin conjugated with Alexa Fluor 647 (T23366, Thermo Fisher Scientific) was reconstituted in H_2O at 5 mg/ml. Cells were washed with Opti-MEM I (without FCS) twice and pre-incubated with 30 μM Dyngo-4a, Dyngo-Ø, or DMSO in Opti-MEM I for 30 min at 37 °C. Then cells were incubated with 25 μg/ml transferrin^{AF647} and 30 μM Dyngo-4a or Dyngo-Ø in Opti-MEM I at 37 °C for 30 min. Afterward, cells were trypsinized, mixed with DMEM plus 10% FCS, centrifuged at 600 × *g* at 4 °C, and washed once with cold PBS and twice with cold FACS buffer (1% FCS in PBS). To assess background signal, a sample was trypsinized after the pre-incubation, mixed with DMEM plus 10% FCS, and centrifuged at 600 × *g* at 4 °C. Subsequently, cells were washed twice with cold PBS, incubated with transferrin^{AF647} and Dyngo-4a in Opti-MEM I for 30 min on ice, and then washed once with cold PBS and twice with cold FACS buffer. Cells were fixed in 1% paraformaldehyde in FACS buffer prior to analysis. All samples were analyzed by FACS Celesta (BD Biosciences) with $\lambda_{ex/em}$ 633/670 nm. Data analysis was performed with FlowJo version 10 to determine the mean fluorescence intensity. The statistics are based on three separately prepared samples.

Immunoprecipitation

50 μl of Dynabeads M-280 sheep anti-mouse or sheep anti-rabbit (Life Technologies) were washed with 3 ml of IP buffer (20 mM Tris, 150 mM NaCl, 5 mM $MgCl_2$, pH 7.4) supplemented with 0.1% BSA. Washed beads were incubated in 800 μl of IP buffer with either 2.5 μl of anti-FLAG M2, 2.5 μl of anti-HA, or 5 μl of mouse monoclonal IgG1-κ as isotype control overnight at 4 °C and washed with 3 ml of IP buffer. 8.8×10^6 cells were used for each individual IP. Harvested cells were stored at −80 °C, thawed on ice, and solubilized using IP buffer containing 0.5% NP40 (Sigma-Aldrich/Merck) or 1% digitonin (Millipore/Merck) and 1× HP protease inhibitor mix (Serva) for 1 h at 4 °C. Lysate was centrifuged at 20,000 × *g* for 20 min at 4 °C. Supernatant was incubated with antibody-coated beads for 2 h at 4 °C and washed with 3 ml of IP buffer containing 0.05% NP40 or 0.1% digitonin. Proteins were eluted by incubation at 90 °C for 20 min in elution buffer containing 2× SDS sample buffer (125 mM Tris, 4% (w/v) SDS, 4 mM EDTA, 0.02% (w/v) bromphenol blue, 20% (v/v) glycerol, pH 6.8) without reducing agents in 25 mM NaOAc, pH 5.0. Samples were analyzed by 10% SDS-PAGE or 10% Tricine-SDS-PAGE followed by immunoblotting.

Cell-free expression and NMR spectroscopy

Synthesis of TMD0 variants, purification, and NMR spectroscopy were performed as described before (62). In short, ^{15}N-uniformly labeled cf-TMD0 and cf-TMD0$_{D17N}$ were synthesized in a continuous exchange *Escherichia coli*-based cell-free expression system. Proteins were solubilized in 1-myristoyl-2-hydroxy-*sn*-glycero-3-(phospho-*rac*-(1-glycerol)) (Avanti Polar Lipids). During immobilized metal affinity chromatography, detergent was exchanged to 1,2-dihexanoyl-*sn*-glycero-3-phosphocholine (c6-DHPC). After elution, buffer was exchanged to NMR sample buffer (25 mM NaOAc, 100 mM NaCl, 0.75% c6-DHPC, 1× HP protease inhibitor mix, pH 5.0). ^{15}N,^{1}H BEST-TROSY NMR spectra of 160 μM of cf-TMD0 and 220 μM of cf-TMD0$_{D17N}$ were recorded at sample temperatures of 313 K on a 700-MHz Bruker AvIII HD spectrometer equipped with a cryogenic ^{1}H/^{31}P/^{13}C/^{15}N quadruple resonance probe.

Peptide transport

40×10^6 HeLa Flp-In T-Rex cells were washed with 60 ml of PBS, harvested by centrifugation for 10 min at 1000 × *g* and 4 °C, and stored at −80 °C. For membrane preparation, cells were thawed on ice, resuspended in Tris buffer (20 mM Tris, 1 mM DTT, 2.5 mM benzamidine, 1 mM PMSF, pH 7.4) and disrupted by Dounce homogenization (40 times) with a tissue grinder (Wheaton). Sucrose was added to a final concentration of 250 mM, and cells were Dounce-homogenized again (10 times). Cell lysate was sequentially centrifuged for 4 min at 200 × *g* and 8 min at 700 × *g* at 4 °C. Subsequently, supernatant was pelleted for 45 min at 100,000 × *g* and 4 °C. Crude membranes were resuspended in PBS, and aliquots were snap-frozen

in liquid nitrogen and stored at −80 °C. Protein concentration in membranes was determined by a Bradford assay (Thermo Fisher Scientific). For peptide transport, crude membranes (120 μg of protein) were incubated in 50 μl of PBS supplemented with 3 mM $MgCl_2$ and 3 μM NST-F (RRYQNSTC$_{Fluorescein}$L) peptide. Peptide transport was started by the addition of 3 mM ATP for 12 min at 37 °C. Transport was stopped with 1 ml of ice-cold stop buffer (PBS supplemented with 10 mM EDTA). Membranes were collected on microfilter plates (MultiScreen plates, Durapore Membrane, 1.2-μm pore size; Merck) preincubated with 0.3% (w/v) polyethyleneimine. Filters were washed three times with 250 μl of ice-cold stop buffer and incubated at room temperature for 10 min in lysis buffer (PBS, 1% SDS, pH 7.5). The amount of transported peptides was analyzed on a fluorescence plate reader (CLARIOstar, BMG LABTECH) at $\lambda_{ex/em}$ = 485/520 nm. ATP-dependent peptide accumulation in crude membranes from nontransfected cells was subtracted, and transport was normalized to TAPL amount determined by immunoblot.

MS-based proteomics

Anti-HA-immunoprecipitation was performed as described previously (22, 63–65). Briefly, expression of TAPL-HA and coreTAPL-HA was induced by the addition of 4 μg/ml doxycycline for 24 h in HeLa Flp-In T-REx cells. Parental nontransfected HeLa Flp-In T-REx cells were used as negative control. For each sample, 6.4×10^7 cells were harvested, frozen in liquid nitrogen, and stored at −80 °C. Cells were lysed in 3 ml of MCLB buffer (50 mM Tris, 150 mM NaCl, 0.5% NP40, pH 7.4) supplemented with cOmplete EDTA-free protease inhibitor tablets (Roche Applied Science, 2 tablets for 50 ml of MCLB buffer) on ice for 30 min. Lysate was cleared by centrifugation (18,000 × *g*, 10 min, 4 °C) followed by filtering through a 0.45-μm spin filter (Millipore). For isolation of HA-tagged proteins, cell lysate was incubated overnight at 4 °C with 60 μl of equilibrated α-HA-agarose beads (Sigma-Aldrich/Merck). Subsequently, beads were washed four times with 1 ml of MCLB and 1 ml of PBS, respectively. 50 μl of 250 μg/ml HA peptide was added to dry beads and incubated for 30 min at room temperature. Elution was repeated twice, obtaining a final volume of 150 μl. Proteins were precipitated with 20% TCA, resuspended in 20 μl of 50 mM ammonium bicarbonate, pH 8.0, containing 10% acetonitrile and 750 ng trypsin (Promega), and incubated for 4 h at 37 °C. Desalting was performed using stage tips. Samples were analyzed as technical duplicates on a LTQ Velos mass spectrometer (Thermo Fisher Scientific), and spectra were identified by Sequest searches as described previously (66). For CompPASS analysis, the identified peptides were compared with IP-MS data of 99 unrelated bait proteins, which were previously processed using the same experimental conditions (22), to obtain weighted and normalized D scores (WD^N score). Proteins with $WD^N \geq 1.0$ and APSM (average peptide spectral matches) ≥ 4 were considered as high-confidence candidate interacting proteins. To account for co-purifying (background) proteins in HeLa cells and coreTAPL-binding proteins, proteins found in these two IP conditions were subtracted from the list of TAPL HCIPs. The MS proteomics data have been deposited to the ProteomeXchange Consortium via the PRIDE (67) partner repository with the data set identifier PXD010989.

Author contributions—P. G. and R. A. conceptualization; P. G., C. Bock, K. W., A. H., N. K., M. B., J. J., F. L., and C. Behrends investigation; P. G. and R. A. writing-original draft; P. G., R. T., and R. A. writing-review and editing; R. A. supervision; R. A. funding acquisition.

Acknowledgments—We thank Inga Nold and Andrea Pott for proofreading the manuscript and Gaby Schneider for advice on statistical analysis.

References

1. Thomas, C., and Tampé, R. (2018) Multifaceted structures and mechanisms of ABC transport systems in health and disease. *Curr. Opin. Struct. Biol.* **51,** 116–128 CrossRef Medline
2. ter Beek, J., Guskov, A., and Slotboom, D. J. (2014) Structural diversity of ABC transporters. *J. Gen. Physiol.* **143,** 419–435 CrossRef Medline
3. Wolters, J. C., Abele, R., and Tampé, R. (2005) Selective and ATP-dependent translocation of peptides by the homodimeric ATP binding cassette transporter TAP-like (ABCB9). *J. Biol. Chem.* **280,** 23631–23636 CrossRef Medline
4. Ortmann, B., Androlewicz, M. J., and Cresswell, P. (1994) MHC class I/β2-microglobulin complexes associate with TAP transporters before peptide binding. *Nature* **368,** 864–867 CrossRef Medline
5. Blees, A., Januliene, D., Hofmann, T., Koller, N., Schmidt, C., Trowitzsch, S., Moeller, A., and Tampé, R. (2017) Structure of the human MHC-I peptide-loading complex. *Nature* **551,** 525–528 CrossRef Medline
6. Zhang, F., Zhang, W., Liu, L., Fisher, C. L., Hui, D., Childs, S., Dorovini-Zis, K., and Ling, V. (2000) Characterization of ABCB9, an ATP binding cassette protein associated with lysosomes. *J. Biol. Chem.* **275,** 23287–23294 CrossRef Medline
7. Demirel, Ö., Waibler, Z., Kalinke, U., Grünebach, F., Appel, S., Brossart, P., Hasilik, A., Tampé, R., and Abele, R. (2007) Identification of a lysosomal peptide transport system induced during dendritic cell development. *J. Biol. Chem.* **282,** 37836–37843 CrossRef Medline
8. Lawand, M., Evnouchidou, I., Baranek, T., Montealegre, S., Tao, S., Drexler, I., Saveanu, L., Si-Tahar, M., and van Endert, P. (2018) Impact of the TAP-like transporter in antigen presentation and phagosome maturation. *Mol. Immunol.* S0161–5890(18)30483–8 CrossRef Medline
9. Kawai, H., Tanji, T., Shiraishi, H., Yamada, M., Iijima, R., Inoue, T., Kezuka, Y., Ohashi, K., Yoshida, Y., Tohyama, K., Gengyo-Ando, K., Mitani, S., Arai, H., Ohashi-Kobayashi, A., and Maeda, M. (2009) Normal formation of a subset of intestinal granules in *Caenorhabditis elegans* requires ATP-binding cassette transporters HAF-4 and HAF-9, which are highly homologous to human lysosomal peptide transporter TAP-like. *Mol. Biol. Cell* **20,** 2979–2990 CrossRef Medline
10. Kamakura, A., Fujimoto, Y., Motohashi, Y., Ohashi, K., Ohashi-Kobayashi, A., and Maeda, M. (2008) Functional dissection of transmembrane domains of human TAP-like (ABCB9). *Biochem. Biophys. Res. Commun.* **377,** 847–851 CrossRef Medline
11. Demirel, Ö., Bangert, I., Tampé, R., and Abele, R. (2010) Tuning the cellular trafficking of the lysosomal peptide transporter TAPL by its N-terminal domain. *Traffic* **11,** 383–393 CrossRef Medline
12. Demirel Ö., Jan, I., Wolters, D., Blanz, J., Saftig, P., Tampé, R., and Abele, R. (2012) The lysosomal polypeptide transporter TAPL is stabilized by interaction with LAMP-1 and LAMP-2. *J. Cell Sci.* **125,** 4230–4240 CrossRef Medline
13. Braulke, T., and Bonifacino, J. S. (2009) Sorting of lysosomal proteins. *Biochim. Biophys. Acta* **1793,** 605–614 CrossRef Medline
14. Hunziker, W., and Geuze, H. J. (1996) Intracellular trafficking of lysosomal membrane proteins. *Bioessays* **18,** 379–389 CrossRef Medline
15. Staudt, C., Puissant, E., and Boonen, M. (2016) Subcellular trafficking of mammalian lysosomal proteins: an extended view. *Int. J. Mol. Sci.* **18,** E47 CrossRef Medline

16. Boncompain, G., Divoux, S., Gareil, N., de Forges, H., de Lescure, A., Latreche, L., Mercanti, V., Jollivet, F., Raposo, G., and Perez, F. (2012) Synchronization of secretory protein traffic in populations of cells. *Nat. Methods* **9,** 493–498 CrossRef Medline
17. McCluskey, A., Daniel, J. A., Hadzic, G., Chau, N., Clayton, E. L., Mariana, A., Whiting, A., Gorgani, N. N., Lloyd, J., Quan, A., Moshkanbaryans, L., Krishnan, S., Perera, S., Chircop, M., von Kleist, L., *et al.* (2013) Building a better dynasore: the dyngo compounds potently inhibit dynamin and endocytosis. *Traffic* **14,** 1272–1289 CrossRef Medline
18. Motley, A., Bright, N. A., Seaman, M. N. J., and Robinson, M. S. (2003) Clathrin-mediated endocytosis in AP-2–depleted cells. *J. Cell Biol.* **162,** 909–918 CrossRef Medline
19. Harding, C., Heuser, J., and Stahl, P. (1983) Receptor-mediated endocytosis of transferrin and recycling of the transferrin receptor in rat reticulocytes. *J. Cell Biol.* **97,** 329–339 CrossRef Medline
20. Bock, C., Löhr, F., Tumulka, F., Reichel, K., Würz, J., Hummer, G., Schäfer, L., Tampé, R., Joseph, B., Bernhard, F., Dötsch, V., and Abele, R. (2018) Structural and functional insights into the interaction and targeting hub TMD0 of the polypeptide transporter TAPL. *Sci. Rep.* **8,** 15662 CrossRef Medline
21. Kobayashi, A., Kasano, M., Maeda, T., Hori, S., Motojima, K., Suzuki, M., Fujiwara, T., Takahashi, E., Yabe, T., Tanaka, K., Kasahara, M., Yamaguchi, Y., and Maeda, M. (2000) A half-type ABC transporter TAPL is highly conserved between rodent and man, and the human gene is not responsive to interferon-γ in contrast to TAP1 and TAP2. *J. Biochem.* **128,** 711–718 CrossRef Medline
22. Sowa, M. E., Bennett, E. J., Gygi, S. P., and Harper, J. W. (2009) Defining the human deubiquitinating enzyme interaction landscape. *Cell* **138,** 389–403 CrossRef Medline
23. Alterio, J., Masson, J., Diaz, J., Chachlaki, K., Salman, H., Areias, J., Al Awabdh, S., Emerit, M. B., and Darmon, M. (2015) Yif1B is Involved in the anterograde traffic pathway and the Golgi architecture. *Traffic* **16,** 978–993 CrossRef Medline
24. Kuijpers, M., Yu, K. L., Teuling, E., Akhmanova, A., Jaarsma, D., and Hoogenraad, C. C. (2013) The ALS8 protein VAPB interacts with the ER-Golgi recycling protein YIF1A and regulates membrane delivery into dendrites. *EMBO J.* **32,** 2056–2072 CrossRef Medline
25. Kiss, K., Kucsma, N., Brozik, A., Tusnady, G. E., Bergam, P., van Niel, G., and Szakacs, G. (2015) Role of the N-terminal transmembrane domain in the endo-lysosomal targeting and function of the human ABCB6 protein. *Biochem. J.* **467,** 127–139 CrossRef Medline
26. Chen, Y., Gershlick, D. C., Park, S. Y., and Bonifacino, J. S. (2017) Segregation in the Golgi complex precedes export of endolysosomal proteins in distinct transport carriers. *J. Cell Biol.* **216,** 4141–4151 CrossRef Medline
27. Nie, C., Wang, H., Wang, R., Ginsburg, D., and Chen, X.-W. (2018) Dimeric sorting code for concentrative cargo selection by the COPII coat. *Proc. Natl. Acad. Sci. U.S.A.* **115,** E3155–E3162 CrossRef Medline
28. Stevenson, N. L., Bergen, D. J. M., Skinner, R. E. H., Kague, E., Martin-Silverstone, E., Robson Brown, K. A., Hammond, C. L., and Stephens, D. J. (2017) Giantin-knockout models reveal a feedback loop between Golgi function and glycosyltransferase expression. *J. Cell Sci.* **130,** 4132–4143 CrossRef Medline
29. Kent, H. M., Evans, P. R., Schäfer, I. B., Gray, S. R., Sanderson, C. M., Luzio, J. P., Peden, A. A., and Owen, D. J. (2012) Structural basis of the intracellular sorting of the SNARE VAMP7 by the AP3 adaptor complex. *Dev. Cell* **22,** 979–988 CrossRef Medline
30. Pak, Y., Glowacka, W. K., Bruce, M. C., Pham, N., and Rotin, D. (2006) Transport of LAPTM5 to lysosomes requires association with the ubiquitin ligase Nedd4, but not LAPTM5 ubiquitination. *J. Cell Biol.* **175,** 631–645 CrossRef Medline
31. Busch, J. I., Unger, T. L., Jain, N., Tyler Skrinak, R., Charan, R. A., and Chen-Plotkin, A. S. (2016) Increased expression of the frontotemporal dementia risk factor TMEM106B causes C9orf72-dependent alterations in lysosomes. *Hum. Mol. Genet.* **25,** 2681–2697 CrossRef Medline
32. Lang, C. M., Fellerer, K., Schwenk, B. M., Kuhn, P.-H., Kremmer, E., Edbauer, D., Capell, A., and Haass, C. (2012) Membrane orientation and subcellular localization of transmembrane protein 106B (TMEM106B), a major risk factor for frontotemporal lobar degeneration. *J. Biol. Chem.* **287,** 19355–19365 CrossRef Medline
33. Cosson, P., Perrin, J., and Bonifacino, J. S. (2013) Anchors aweigh: protein localization and transport mediated by transmembrane domains. *Trends Cell Biol.* **23,** 511–517 CrossRef Medline
34. Alcover, A., Mariuzza, R. A., Ermonval, M., and Acuto, O. (1990) Lysine 271 in the transmembrane domain of the T-cell antigen receptor β chain is necessary for its assembly with the CD3 complex but not for α/β dimerization. *J. Biol. Chem.* **265,** 4131–4135 Medline
35. Blumberg, R. S., Alarcon, B., Sancho, J., McDermott, F. V., Lopez, P., Breitmeyer, J., and Terhorst, C. (1990) Assembly and function of the T cell antigen receptor: requirement of either the lysine or arginine residues in the transmembrane region of the α chain. *J. Biol. Chem.* **265,** 14036–14043 Medline
36. Kawaguchi, K., Okamoto, T., Morita, M., and Imanaka, T. (2016) Translocation of the ABC transporter ABCD4 from the endoplasmic reticulum to lysosomes requires the escort protein LMBD1. *Sci. Rep.* **6,** 30183 CrossRef Medline
37. Elliott, E. A., Drake, J. R., Amigorena, S., Elsemore, J., Webster, P., Mellman, I., and Flavell, R. A. (1994) The invariant chain is required for intracellular transport and function of major histocompatibility complex class II molecules. *J. Exp. Med.* **179,** 681–694 CrossRef Medline
38. Castellino, F., and Germain, R. N. (1995) Extensive trafficking of MHC class II-invariant chain complexes in the endocytic pathway and appearance of peptide-loaded class II in multiple compartments. *Immunity* **2,** 73–88 CrossRef Medline
39. Roche, P. A., and Cresswell, P. (1990) Invariant chain association with HLA-DR molecules inhibits immunogenic peptide binding. *Nature* **345,** 615–618 CrossRef Medline
40. Odorizzi, C. G., Trowbridge, I. S., Xue, L., Hopkins, C. R., Davis, C. D., and Collawn, J. F. (1994) Sorting signals in the MHC class II invariant chain cytoplasmic tail and transmembrane region determine trafficking to an endocytic processing compartment. *J. Cell Biol.* **126,** 317–330 CrossRef Medline
41. Carrel, D., Masson, J., Al Awabdh, S., Capra, C. B., Lenkei, Z., Hamon, M., Emerit, M. B., and Darmon, M. (2008) Targeting of the 5-HT1A serotonin receptor to neuronal dendrites is mediated by Yif1B. *J. Neurosci.* **28,** 8063–8073 CrossRef Medline
42. Harter, C., and Mellman, I. (1992) Transport of the lysosomal membrane glycoprotein lgp120 (lgp-A) to lysosomes does not require appearance on the plasma membrane. *J. Cell Biol.* **117,** 311–325 CrossRef Medline
43. Höning, S., Griffith, J., Geuze, H. J., and Hunziker, W. (1996) The tyrosine-based lysosomal targeting signal in lamp-1 mediates sorting into Golgi-derived clathrin-coated vesicles. *EMBO J.* **15,** 5230–5239 CrossRef Medline
44. Peden, A. A., Oorschot, V., Hesser, B. A., Austin, C. D., Scheller, R. H., and Klumperman, J. (2004) Localization of the AP-3 adaptor complex defines a novel endosomal exit site for lysosomal membrane proteins. *J. Cell Biol.* **164,** 1065–1076 CrossRef Medline
45. Janvier, K., and Bonifacino, J. S. (2005) Role of the endocytic machinery in the sorting of lysosome-associated membrane proteins. *Mol. Biol. Cell* **16,** 4231–4242 CrossRef Medline
46. Pols, M. S., van Meel, E., Oorschot, V., ten Brink, C., Fukuda, M., Swetha, M. G., Mayor, S., and Klumperman, J. (2013) hVps41 and VAMP7 function in direct TGN to late endosome transport of lysosomal membrane proteins. *Nat. Commun.* **4,** 1361 CrossRef Medline
47. Karlsson, K., and Carlsson, S. R. (1998) Sorting of lysosomal membrane glycoproteins lamp-1 and lamp-2 into vesicles distinct from mannose 6-phosphate receptor/γ-adaptin vesicles at the *trans*-Golgi network. *J. Biol. Chem.* **273,** 18966–18973 CrossRef Medline
48. Blees, A., Reichel, K., Trowitzsch, S., Fisette, O., Bock, C., Abele, R., Hummer, G., Schäfer, L. V., and Tampé, R. (2015) Assembly of the MHC I peptide-loading complex determined by a conserved ionic lock-switch. *Sci. Rep.* **5,** 17341 CrossRef Medline
49. Abacioglu, Y. H., Fouts, T. R., Laman, J. D., Claassen, E., Pincus, S. H., Moore, J. P., Roby, C. A., Kamin-Lewis, R., and Lewis, G. K. (1994) Epitope mapping and topology of baculovirus-expressed HIV-1 gp160 determined

with a panel of murine monoclonal antibodies. *AIDS Res. Hum. Retroviruses* **10,** 371–381 CrossRef Medline
50. Zollmann, T., Moiset, G., Tumulka, F., Tampé, R., Poolman, B., and Abele, R. (2015) Single liposome analysis of peptide translocation by the ABC transporter TAPL. *Proc. Natl. Acad. Sci. U.S.A.* **112,** 2046–2051 CrossRef Medline
51. Ran, F. A., Hsu, P. D., Wright, J., Agarwala, V., Scott, D. A., and Zhang, F. (2013) Genome engineering using the CRISPR-Cas9 system. *Nat. Protoc.* **8,** 2281–2308 CrossRef Medline
52. Schägger, H., and von Jagow, G. (1987) Tricine-sodium dodecyl sulfate-polyacrylamide gel electrophoresis for the separation of proteins in the range from 1 to 100 kDa. *Anal. Biochem.* **166,** 368–379 CrossRef Medline
53. Burnette, W. N. (1981) "Western blotting": electrophoretic transfer of proteins from sodium dodecyl sulfate–polyacrylamide gels to unmodified nitrocellulose and radiographic detection with antibody and radioiodinated protein A. *Anal. Biochem.* **112,** 195–203 CrossRef Medline
54. The UniProt Consortium (2017) UniProt: the universal protein knowledgebase. *Nucleic Acids Res.* **45,** D158–D169 CrossRef Medline
55. Edgar, R. C. (2004) MUSCLE: multiple sequence alignment with high accuracy and high throughput. *Nucleic Acids Res.* **32,** 1792–1797 CrossRef Medline
56. Li, W., Cowley, A., Uludag, M., Gur, T., McWilliam, H., Squizzato, S., Park, Y. M., Buso, N., and Lopez, R. (2015) The EMBL-EBI bioinformatics web and programmatic tools framework. *Nucleic Acids Res.* **43,** W580–W584 CrossRef Medline
57. Schindelin, J., Arganda-Carreras, I., Frise, E., Kaynig, V., Longair, M., Pietzsch, T., Preibisch, S., Rueden, C., Saalfeld, S., Schmid, B., Tinevez, J.-Y., White, D. J., Hartenstein, V., Eliceiri, K., Tomancak, P., and Cardona, A. (2012) Fiji: an open-source platform for biological-image analysis. *Nat. Methods* **9,** 676–682 CrossRef Medline
58. Schneider, C. A., Rasband, W. S., and Eliceiri, K. W. (2012) NIH Image to ImageJ: 25 years of image analysis. *Nat. Methods* **9,** 671–675 CrossRef Medline
59. Kirshner, H., Aguet, F., Sage, D., and Unser, M. (2013) 3-D PSF fitting for fluorescence microscopy: implementation and localization application. *J. Microsc.* **249,** 13–25 CrossRef Medline
60. Sage, D., Donati, L., Soulez, F., Fortun, D., Schmit, G., Seitz, A., Guiet, R., Vonesch, C., and Unser, M. (2017) DeconvolutionLab2: an open-source software for deconvolution microscopy. *Methods* **115,** 28–41 CrossRef Medline
61. Robertson, M. J., Deane, F. M., Robinson, P. J., and McCluskey, A. (2014) Synthesis of Dynole 34-2, Dynole 2-24 and Dyngo 4a for investigating dynamin GTPase. *Nat. Protoc.* **9,** 851–870 CrossRef Medline
62. Tumulka, F., Roos, C., Löhr, F., Bock, C., Bernhard, F., Dötsch, V., and Abele, R. (2013) Conformational stabilization of the membrane embedded targeting domain of the lysosomal peptide transporter TAPL for solution NMR. *J. Biomol. NMR* **57,** 141–154 CrossRef Medline
63. Behrends, C., Sowa, M. E., Gygi, S. P., and Harper, J. W. (2010) Network organization of the human autophagy system. *Nature* **466,** 68–76 CrossRef Medline
64. Jung, J., Genau, H. M., and Behrends, C. (2015) Amino acid-dependent mTORC1 regulation by the lysosomal membrane protein SLC38A9. *Mol. Cell Biol.* **35,** 2479–2494 CrossRef Medline
65. Jung, J., Nayak, A., Schaeffer, V., Starzetz, T., Kirsch, A. K., Müller, S., Dikic, I., Mittelbronn, M., and Behrends, C. (2017) Multiplex image-based autophagy RNAi screening identifies SMCR8 as ULK1 kinase activity and gene expression regulator. *Elife* **6,** e23063 CrossRef Medline
66. Huttlin, E. L., Jedrychowski, M. P., Elias, J. E., Goswami, T., Rad, R., Beausoleil, S. A., Villén, J., Haas, W., Sowa, M. E., and Gygi, S. P. (2010) A tissue-specific atlas of mouse protein phosphorylation and expression. *Cell* **143,** 1174–1189 CrossRef Medline
67. Vizcaíno, J. A., Csordas, A., del-Toro, N., Dianes, J. A., Griss, J., Lavidas, I., Mayer, G., Perez-Riverol, Y., Reisinger, F., Ternent, T., Xu, Q.-W., Wang, R., and Hermjakob, H. (2016) 2016 update of the PRIDE database and its related tools. *Nucleic Acids Res.* **44,** D447–D456 CrossRef Medline